Russian Geology and Geophysics © 2020, V.S. Sobolev IGM, Siberian Branch of the RAS
Vol. 61, No. 3, pp. 286–302, 2020 DOI:10.15372/RGG2019095 *Geologiya i Geofizika*

Geochemistry of Metasedimentary Rocks, Sources of Clastic Material, and Tectonic Nature of Mesozoic Basins on the Northern Framing of the Eastern Mongol–Okhotsk Orogenic Belt

V.A. Zaika[a, ✉], A.A. Sorokin[a], V.P. Kovach[b], A.B. Kotov[b]

[a] *Institute of Geology and Nature Management, Far Eastern Branch of the Russian Academy of Sciences, per. Relochnyi 1, Blagoveshchensk, 675000, Russia*

[b] *Institute of the Precambrian Geology and Geochronology, Russian Academy of Sciences, nab. Makarova 2, St. Petersburg, 199034, Russia*

Received 7 November 2018; received in revised form 7 February 2019; accepted 21 March 2019

Abstract—We present results of geochemical studies of the upper Mesozoic deposits of the Strelka and Malaya Tynda depressions and U–Th–Pb (LA-ICP-MS) geochronological and Lu–Hf isotope-geochemical studies of detrital zircons from these deposits. It is shown that the Strelka and Malaya Tynda depressions, adjacent to the Mongol–Okhotsk Orogenic Belt in the north and extending along the boundary between the southern framing of the North Asian Craton and the orogenic belt, are marginal troughs. These troughs are filled with thick beds of Mesozoic marine (at the bottom) and continental (at the top) metaterrigenous rocks, with an increase in the grain size of clastic material up the section; the rocks should be regarded as molasses. The results of U–Th–Pb geochronological studies of detrital zircons from metaterrigenous rocks of the Strelka and Lesser Tynda depressions, on the one hand, and the eastern part of the Mongol–Okhotsk Orogenic Belt, on the other, show that orogenic processes in the east of the belt were completed at the Early–Middle Jurassic boundary. The depressions began to form after the complete closure of the Mongol–Okhotsk basin and the formation of an orogenic structure at its place. Then they were filled with material supplied both from the Selenga–Stanovoi and Dzhugdzhur–Stanovoi superterranes on the southern framing of the North Asian Craton and from the Mongol–Okhotsk Belt, which was a mountain-folded structure in the Middle Jurassic.

Keywords: Mesozoic depressions, sedimentary rocks, detrital zircons, sources, U–Th–Pb method, Lu–Hf method

INTRODUCTION

The Mongol–Okhotsk Orogenic Belt is among the largest structures in Central and East Asia (Fig. 1). It is usually considered to be a relic of the Mongol–Okhotsk Paleo-Ocean, which closed as a result of the collision of the North Asian Craton with the Amur superterrane. At present, the belt is a complex collage of tectonic blocks stretching along its strike, which are regarded as accretionary-wedge terranes (Parfenov et al., 1999; Khanchuk, 2006; Khanchuk et al., 2015).

The available paleomagnetic data (Metelkin et al., 2004, 2007; Didenko et al., 2010; Khanchuk et al., 2015) point to the existence of space between the southern margin of the North Asian Craton and the continental massifs of the southern framing of the Mongol–Okhotsk Belt in the Paleozoic. These data, as well as the presence of Paleozoic and early Mesozoic igneous complexes within the belt and in the framing continental structures (Kozlov et al., 2003; Sorokin et al., 2003, 2005, 2007; Sal'nikova et al., 2006; Buchko et al., 2010, 2018; Tsygankov et al., 2010; Larin et al., 2011; Donskaya et al., 2012, 2013; Sun et al., 2013; Tang et al., 2016; Wang et al., 2017), indicate a long and intricate history of its formation.

Although the Mongol–Okhotsk Orogenic Belt attracts the attention of several generations of geologists, many crucial issues of its evolution have not been resolved yet. The most debatable issues are the time and nature of accretion and collision processes that took place throughout its geologic evolution. Taking into account that the youngest paleo-oceanic deposits of the Mongol–Okhotsk Belt are spread in its eastern part and are dated at the Early Jurassic–Early Middle Jurassic (Parfenov et al., 1999), it is reasonable to assume that orogenic processes (at least in this part of the belt) began in the Early Jurassic (Parfenov et al., 1999). On the other hand, there is a common viewpoint stating that the Mongol–Okhotsk Paleo-Ocean closed in the Early Cretaceous. The ocean closure is associated with metamorphic processes within the northern (Larin et al., 2006; Sal'nikova et al., 2006; Donskaya et al., 2008, 2012; Kotov et al., 2012; et al.) and southern (Kotov et al., 2009, 2013, 2014; Larin et al., 2014) continental margins of the belt and with intraplate magmatism (Donskaya et al., 2013). Collision at the Late Jurassic–Early Cretaceous boundary is assumed based on

✉ Corresponding author.
E-mail address: zaikava@ignm.ru (V.A. Zaika)

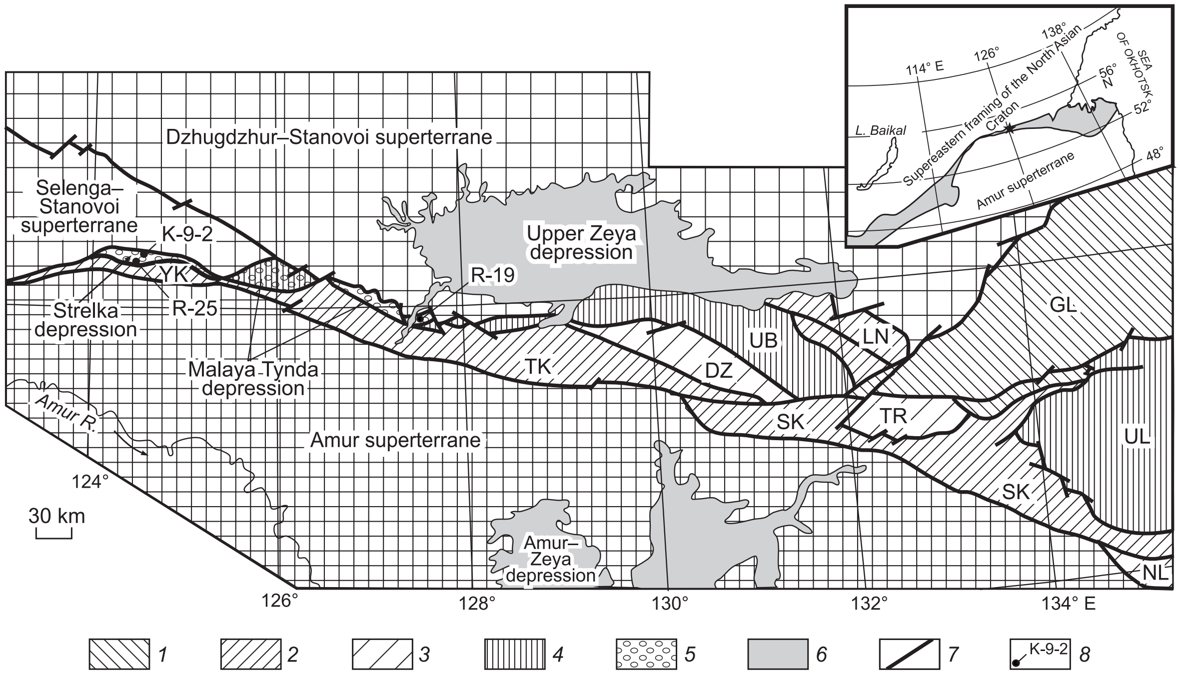

Fig. 1. Schematic structural regionalization of the eastern part of the Mongol–Okhotsk Orogenic Belt (Sorokin et al., 2003). *1*, terranes composed mostly of lower and middle Paleozoic metasedimentary and metavolcanic rocks; *2*, terranes composed mostly of middle and upper Paleozoic metasedimentary and metavolcanic complexes; *3*, terranes composed mostly of upper Paleozoic metasedimentary and metavolcanic rocks; *4*, terranes composed mostly of lower Mesozoic turbidite rocks; *5*, Upper Jurassic–Lower Cretaceous conglomerates, gritstones, and sandstones; *6*, Cenozoic loose sediments; *7*, faults; *8*, localities of sampling for geochemical, isotope-geochemical, and geochronological studies and their numbers. The study area is asterisked in the inset. Gray field is the Mongol–Okhotsk Orogenic Belt. Terranes: GL, Galam; DZ, Dzhagdy; LN, Lan; SK, Selemdzha–Kerbi; TK, Tukuringra; TR, Tokur; UL, Ul'ban; UB, Un'ya–Bom; YK, Yankan; Nl, Nilan.

the evolution of sedimentary basins in East Asia (Yang et al., 2015; Guo et al., 2017), and the paleomagnetic data also point to an Early Cretaceous age of collision processes (Zhao et al., 1994; Kravchinsky et al., 2002; Metelkin et al., 2004, 2007, 2010; Ren et al., 2016). Analysis of seismic anomalies also indicates an Early Cretaceous age of the Mongol–Okhotsk Ocean (Wu et al., 2017).

The information about the age, provenances, and tectonic conditions of accumulation of terrigenous rocks of the Mesozoic sedimentary basins located within the continental framing structures of the Mongol–Okhotsk Belt can help to clarify the age of collision during the belt formation. For example, the results of recent Sm–Nd isotope-geochemical studies of the Jurassic terrigenous rocks of the Irkutsk sedimentary basin and of U–Pb dating of the hosted detrital zircons show that the orogenic processes related to the closure of the western part of the Mongol–Okhotsk Ocean began at the Early–Middle Jurassic boundary (Demonterova et al., 2017). In the south, the eastern part of the belt borders upon the Upper Amur and Zeya–Dep troughs filled with Jurassic terrigenous deposits. The structure of these troughs, typical of foreland basins (Smirnova et al., 2017), the presence of coal horizons in the Middle–Upper Jurassic deposits (Resolutions..., 1994), and the chemical composition of sedimentary rocks of the deposits indicate that orogenic processes in the east of the Mongol–Okhotsk Belt began before the Middle Jurassic (Smirnova et al., 2017).

The importance of clarifying the age of the closure of the Mongol–Okhotsk Ocean and the formation of an Orogenic Belt at its place forced us to study two more objects, namely, the Strelka and Malaya Tynda depressions. In the north, these depressions border upon the eastern part of the Mongol–Okhotsk Orogenic Belt (Fig. 1) and are composed of Late Jurassic–Early Cretaceous and Early Cretaceous metasedimentary deposits. In this paper we present results of geochemical studies of the upper Mesozoic rocks of these depressions and of U–Th–Pb (LA-ICP-MS) geochronological and Lu–Hf isotope-geochemical studies of their detrital zircons.

GEOLOGY OF THE STUDIED OBJECTS

The Strelka depression extends for ~70 km from east to west, along the boundary between the southern margin of the Selenga–Stanovoi superterrane and the Yankan terrane of the Mongol–Okhotsk Orogenic Belt, with its maximum width of 11–14 km (Fig. 1).

According to known concepts (Koshelenko, 2011), the lower section of the Strelka depression is the 400–1100 m thick Dolokhit Formation including two subformations. The Lower Dolokhit Subformation is composed of sandstones, siltstones, and mudstones. The Upper Dolokhit Subformation is made up mostly of sandstones with scarce interbeds of siltstones, gritstones, and conglomerates. The Middle Jurassic age of the Dolokhit Formation is substantiated by the findings of bivalves *Dacriomya Subjakutica* Polub. and *Meleagrinella* (?) sp. and ammonites *Liostrea* (?) sp. ind. at the bottom of its section. The Dolokhit Formation is overlain with erosion by the Upper Jurassic–Lower Cretaceous Kholodzhikan or Strelka (Serezhnikov and Volkova, 2007; Petruk and Kozlov, 2009) formations 940–2150 m thick. The latter is made up of conglomerates, gritstones, medium- and coarse-grained sandstones, carbonaceous siltstones, and scarce coal interbeds. The formation contains remains of Late Jurassic–Early Cretaceous flora (*Coniopteris* cf. *burejensis* (Lal.), *C. hymenophylloides* (Brongn.), *Cladophlebis aldanensis* Vachr., *C. argutula* (Heer) Font, *C. williamsonii* (Brongn), *C. kamenkensis* Thom., *C. haiburnensis* (L. et H.), *Czekanowskia setacea* Heer., *Cz. rigida* Heer, *Phoenicopsis angustifolia* Heer., *P. speciosa* Heer., *Podosamites lanceolatus* L. et H., *leptostrobus laxiflora* Heer., *Crassoza mites burejensis* Pryn., *Sphenobaiera longfolia*, *Pytiophyllum nordenskioldii* (Heer) Nath., *Equisetites* cf. *ferganensis* Se.).

The deposits of the Strelka depression are intruded by granitoids of the Dzhalinda pluton (125 ± 2 Ma (Koshelenko, 2011)) and dikes of quartz diorite porphyrites and granodiorite porphyry (128–126 Ma (Sorokin et al., 2014)).

The Malaya Tynda depression extends for more than 130 km from east to west, along the boundary between the Dzhugdzhur–Stanovoi superterrane in the north and the Tukuringra terrane of the Mongol–Okhotsk Orogenic Belt in the south, with its maximum width of 10–15 km (Fig. 1). Its lower section is composed of phyllitized siltstones with interbeds of sandstones and mudstones and lenses of conglomerates and carbonaceous shales of the 1120 m thick Middle Jurassic Dess Formation (Serezhnikov and Volkova, 2007; Petruk and Kozlov, 2009). The siltstones were found to contain *Mytiloceramus ambiguus* (Eichw.), *M.* cf. *formosolus* (Vor.) Sey, *M.* cf. *ussuriensis* (Vor.) Sey, *M.* cf. *lucifer* (Eichw.), and *M.* cf. *jurensis* (Kosch.) of Aalenian–Bajocian age (Serezhnikov and Volkova, 2007). The Middle Jurassic Dess Formation is overlain with erosion by boulder–pebble conglomerates with interbeds of polymict sandstones, arkoses, gritstones, and carbonaceous siltstones of the Upper Jurassic–Lower Cretaceous Kholodzhikan (Godzevich, 1984; Vol'skii et al., 2014) or Strelka (Serezhnikov and Volkova, 2007; Petruk and Kozlov, 2009) formations. In the Malaya Tynda depression, the Kholodzhikan Formation is >1500 m in thickness and contains abundant plant remains, including Jurassic *Raphaelia* cf. *diamensis* Sew. The presence of equiseta *Equisetites tschetschumensis* Vas. typical of the Chechum Horizon of the Lena basin gives grounds to limit the age of the top of the formation to the Tithonian (Late Jurassic) (Serezhnikov and Volkova, 2007). The Mesozoic section of the depression is crowned with boulder–pebble and pebble conglomerates with interbeds of coarse-grained sandstones, which are united into the 2500 m thick Lower Cretaceous Malaya Tynda Formation. These rocks contain fossils of *Ginkgo sibirica* Heer, *Podosamites lanceolatus* L. et H., and *Pituophyllum nordenskioldia* (Heer) of Barremian–Aptian age (Serezhnikov and Volkova, 2007).

The objects of our study were Jurassic rocks of the Upper Dolokhit Subformation in the central zone of the Strelka depression and the Lower Cretaceous rocks of the Malaya Tynda Formation in the eastern part of the Malaya Tynda depression (Fig. 1).

METHODS

The chemical composition of rocks was studied by XRF (major components and Zr) at Institute of Geology and Nature Management, Blagoveshchensk, and by ICP MS (Li, Rb, Sr, Ba, REE, Y, Th, U, Nb, Ta, Pb, Zn, Co, Ni, Sc, V, and Cr) at the Yu.A. Kosygin Institute of Tectonics and Geophysics, Khabarovsk. The powdered samples for XRF analysis were homogenized by fusion with a mixture of $LiBO_2$ + $Li_2B_4O_7$ in a muffle furnace at 1050–1100 ºC. Analyses were made on a Pioneer 4S X-ray spectrometer. The intensity of spectral lines was corrected for background, absorption, and secondary fluorescence. For ICP MS analysis, the samples were subjected to acid digestion. The ICP MS measurements were performed on an Elan 6100 DRC mass spectrometer in the standard regime. Calibration of the mass spectrometer was made using standard solutions containing all elements to be analyzed. The error of measurement of major and trace elements was 5–10 rel.%.

Zircons were separated from the samples at the Mineralogical Laboratory of the IGNM, using heavy liquids. Then, these zircons, along with standard zircon samples (FC, SL, and R33), were implanted into an epoxy resin pellet and polished to nearly the middle of their grains. The internal structure of the zircon grains was examined with a Hitachi S-3400N scanning electron microscope equipped with a Gatan Chroma CL2 detector in the BSE mode. U–Th–Pb geochronological studies of individual zircons were carried out at the Arizona LaserChron Center, USA, using a Photon Machines Analyte G2 laser ablation system and a Thermo Element 2 ICP mass spectrometer. The spot diameter was 20 µm, and the spot depth was 15 µm. Calibration was made against the FC standard zircon (Duluth complex, 1099.3 ± 0.3 Ma (Paces and Miller, 1993)). The SL (Sri Lanka) and R33 (Braintree complex) zircons (Black et al., 2004) were used as secondary standards for measurement control. The average $^{206}Pb/^{238}U$ and $^{207}Pb/^{206}Pb$ ages for the SL standard during the measurements were 557 ± 5 and 558 ± 7 Ma (2σ), respectively, and agreed with the values obtained by ID-TIMS (Gehrels et al., 2008). The average $^{206}Pb/^{238}U$ and $^{207}Pb/^{206}Pb$ ages for the R33 standard were 417 ± 7 and 415 ± 8 Ma and agreed with the earlier documented ones (Black et al., 2004; Mattinson, 2010). The systematic errors were 0.9% for $^{206}Pb/^{238}U$ and 0.8% for $^{206}Pb/^{207}Pb$ (2s). Corrections for terrestrial Pb were introduced based on ^{204}Hg-corrected ^{204}Pb in accordance with model values (Stacey and Kramers, 1975). The following uranium decay constants and uranium isotope ratios were used: $^{238}U = 9.8485 \times 10^{-10}$, $^{235}U = 1.55125 \times 10^{-10}$, $^{238}U/^{235}U = 137.88$. The analytical technique is described in detail on the laboratory website (www.laserchron.org). The concordant ages were calculated using the ISOPLOT program (version 3.6) (Ludwig, 2008).

Lu–Hf isotope analyses of zircons were performed at the Arizona LaserChron Center, USA, using a Nu high-resolution multichannel inductively coupled plasma mass spectrometer (MC-ICP-MS) and an Analyte G2 excimer laser ablation system. The JMC475, Spex Hf, and Spex Yb, and Spex Lu standard solutions and Mud Tank, 91500, Temora, R33, FC52, Plesovice, and SL standard zircons were used to set up instruments and control the quality of analyses. Hf isotope and U–Th–Pb analyses of zircons were carried out at the same sites. The laser used had the following parameters: beam diameter, 40 μm; power, ~5 J/cm^2; frequency, 7 Hz; and ablation rate, ~0.8 μm/s. The standard zircons were analyzed after every 20 zircons under study. The analytical technique is described in detail on www.laserchron.org. The $\varepsilon_{Hf}(t)$ values were calculated using the ^{176}Lu decay constant ($\lambda = 1.867e^{-11}$) (Söderlund et al., 2004) and $^{176}Hf/^{177}Hf$ (0.282785) and $^{176}Lu/^{177}Hf$ (0.0336) of chondrite (Blichert-Toft and Albarède, 1997). The Hf model ages t_{Hf}(C) of the crust were calculated taking the average $^{176}Lu/^{177}Hf$ ratio of the continental crust equal to 0.0093 (Vervoort and Patchett, 1996; Amelin et al., 1999). The isotope parameters of the depleted mantle were evaluated based on the recent $^{176}Hf/^{177}Hf$ and $^{176}Lu/^{177}Hf$ ratios (0.28325 and 0.0384, respectively) (Griffin et al., 2004).

PETROGRAPHY AND GEOCHEMISTRY OF THE ROCKS

Sandstones prevail in our collection of rock samples from the Upper Dolokhit Subformation of the Strelka depression. These are gray medium-grained rocks with a psammitic texture and a massive or, less often, schistose structure. The nongraded clastic material 0.2–0.7 mm in size is mostly angular and semiangular quartz (55–70%) and feldspar (25–35%) grains. There are also fragments of acid rocks, microquartzites, and sericite–quartz schists (up to 10%). The accessory minerals are magnetite, zircon, and garnet. The cement is of contact or contact–pore type.

Conglomerates of the Upper Dolokhit Subformation are composed of well-rounded granite, gneiss, and amphibolite pebble up to 5 cm in size, with the contents of fragments and binding material of 40 and 60%, respectively. The groundmass is gray medium-grained, with a psammitic texture and a massive structure. The prevailing minerals are semiangular and semirounded grains (0.1–1.3 mm in size) of quartz (65–75%) and feldspars (20–30%). There are also fragments of acid rocks and schists (up to 10%). The accessory minerals are garnet, magnetite, zircon, and iron hydroxides. The chemical composition of the samples is presented in Table 1.

Sandstones of the Upper Dolokhit Subformation correspond in the SiO_2/Al_2O_3–Na_2O/K_2O correlation to graywackes. One can see variations in the above ratios and the separate location of two fields of the composition points of the subformation rocks (Fig. 2*a*). These rocks correspond in the SiO_2/Al_2O_3–$Fe_2O_3^*/K_2O$ correlation to wackes. Because

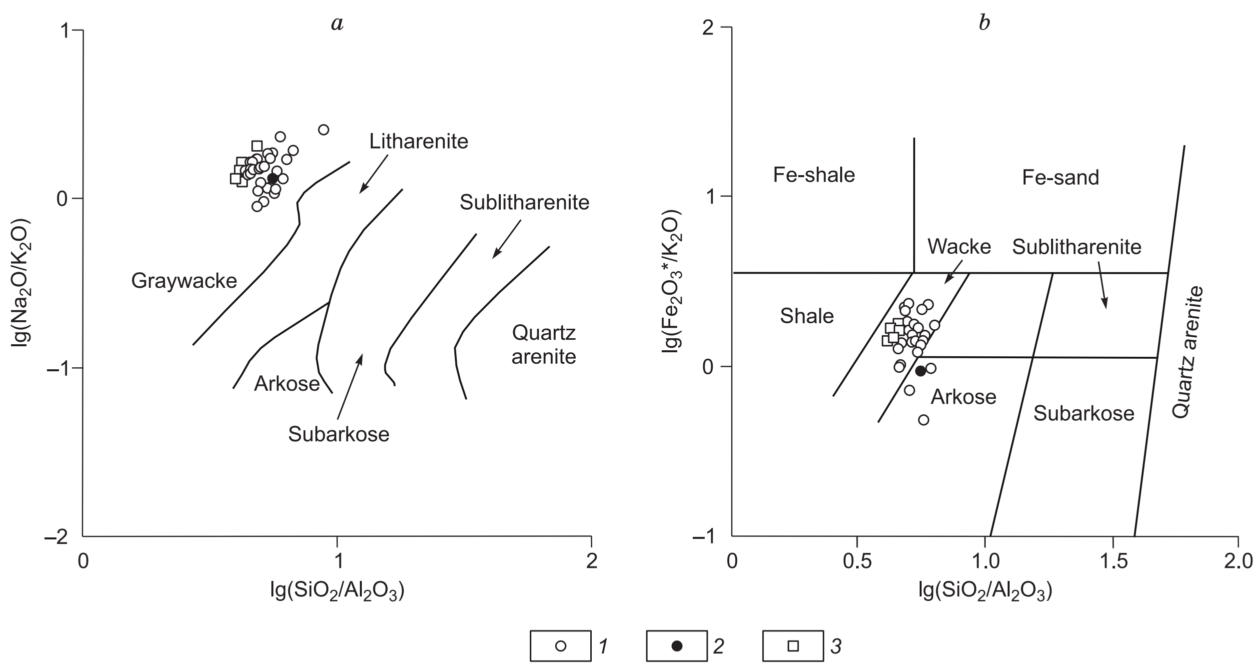

Fig. 2. lg(SiO_2/Al_2O_3)–lg(Na_2O/K_2O) (*a*) (Pettijohn et al., 1972) and lg(SiO_2/Al_2O_3)–lg(Fe_2O_3/K_2O) (*b*) (Herron, 1988) diagrams for metasedimentary rocks of the Strelka and Malaya Tynda depressions. *1*, sandstones of the Upper Dolokhit Subformation of the Strelka depression; *2*, cement of conglomerates of the Upper Dolokhit Subformation; *3*, sandstones of the Malaya Tynda Formation of the Malaya Tynda depression.

Table 1. Chemical composition of representative samples of metasedimentary rocks of the Strelka and Malaya Tynda depressions

Component	R-19	R-19-1	R-19-3	R-19-4	R-19-5	R-25	C-1299	C-1299-1	C-1299-2	C-1299-3	C-1299-4	C-1299-5	C-1299-6	K-9	K-9-1
	1	2	3	4	5	6	7	8	9	10	11	12	13	14	15
SiO_2	65.76	66.96	66.62	65.70	65.65	66.71	69.36	68.48	70.62	68.11	69.36	68.54	68.33	71.54	70.76
TiO_2	0.53	0.30	0.41	0.52	0.45	0.59	0.38	0.46	0.41	0.57	0.45	0.49	0.56	0.51	0.57
Al_2O_3	14.48	13.86	14.54	14.77	15.09	13.37	15.15	14.78	13.69	14.12	14.83	15.10	13.68	13.22	13.00
Fe_2O_3*	4.92	3.73	4.55	4.81	4.40	5.68	3.09	3.08	3.55	4.24	3.66	3.32	4.30	4.17	4.22
MnO	0.08	0.12	0.06	0.07	0.06	0.08	0.05	0.05	0.07	0.07	0.06	0.06	0.07	0.04	0.07
MgO	1.33	1.18	1.31	1.38	1.33	1.51	1.21	1.33	1.15	1.66	1.35	0.96	1.71	1.15	1.15
CaO	3.84	3.91	3.23	3.39	3.21	3.23	1.05	1.98	1.94	2.27	1.67	1.35	2.29	1.10	2.70
Na_2O	4.00	4.78	4.22	4.17	4.38	3.75	4.45	5.02	3.63	4.42	3.99	4.34	3.30	4.04	4.37
K_2O	2.73	2.29	2.77	2.96	2.95	2.40	3.10	2.99	2.30	2.53	2.64	2.59	2.61	3.41	2.48
P_2O_5	0.12	0.09	0.10	0.10	0.10	0.15	0.09	0.11	0.12	0.12	0.11	0.11	0.13	0.12	0.14
LOI	1.41	2.10	1.37	1.37	1.52	1.76	1.55	1.76	1.70	1.80	1.72	3.01	2.03	0.68	0.46
Total	99.20	99.32	99.18	99.24	99.14	99.23	99.48	100.04	99.18	99.91	99.84	99.87	99.01	99.98	99.92
Li	14.9	12.4	17.2	19.0	13.8	22.4	9.7	13.5	14.4	13.1	12.7	15.9	14.5	9.5	20.4
Ga	17.3	14.5	16.7	17.5	18.9	17.3	15.6	16.4	14.5	15.3	14.4	14.2	14.9	17.1	22.3
Rb	55	48	56	62	64	71	73	76	61	62	68	62	64	91	69
Sr	668	608	659	584	506	588	317	333	401	386	298	311	374	399	453
Ba	810	658	819	861	958	829	871	964	928	739	674	671	735	1532	1224
La	32.5	26.4	17.5	28.1	27.1	30.7	18.6	24.5	19.9	30.1	20.8	22.1	32.8	47.3	63.0
Ce	64.4	39.8	35.5	57.1	51.8	61.6	39.7	51.1	43.0	62.8	44.0	46.7	68.3	92.4	118.1
Pr	7.10	5.03	4.03	6.45	5.85	6.93	4.29	5.44	4.58	6.72	4.82	5.02	7.23	9.75	12.42
Nd	25.8	19.2	15.4	23.6	21.5	25.6	16.1	20.3	17.3	25.2	18.2	18.8	26.8	39.3	48.7
Sm	4.34	3.30	2.71	4.12	3.57	4.51	2.81	3.51	3.13	4.38	3.28	3.27	4.64	5.50	7.70
Eu	1.03	1.02	0.85	1.04	0.96	1.09	0.81	1.24	0.83	1.04	0.87	0.69	1.10	0.84	1.56
Gd	4.29	3.43	2.76	4.13	3.37	4.32	2.52	3.06	2.83	3.92	3.08	2.81	4.12	4.50	7.17
Tb	0.50	0.41	0.32	0.47	0.38	0.53	0.36	0.45	0.41	0.56	0.44	0.39	0.58	0.44	0.65
Dy	2.69	2.29	1.76	2.65	2.03	2.87	1.90	2.36	2.23	2.99	2.45	2.05	3.07	2.39	3.70
Ho	0.51	0.44	0.35	0.52	0.37	0.53	0.35	0.43	0.41	0.54	0.45	0.37	0.55	0.34	0.64
Er	1.50	1.25	0.98	1.52	1.06	1.54	1.06	1.30	1.25	1.65	1.34	1.14	1.67	0.92	1.77
Tm	0.20	0.16	0.13	0.20	0.15	0.21	0.14	0.17	0.16	0.22	0.18	0.15	0.22	0.11	0.20
Yb	1.32	1.02	0.85	1.28	0.92	1.33	0.96	1.13	1.11	1.42	1.18	1.02	1.46	0.84	1.33
Lu	0.19	0.15	0.13	0.19	0.13	0.20	0.14	0.16	0.16	0.20	0.17	0.14	0.20	0.12	0.18
Y	12.7	11.6	8.6	12.6	9.6	13.2	8.7	11.0	10.9	14.5	11.9	9.1	14.6	7.9	17.4
Nb	6.96	3.60	4.89	7.12	5.83	6.87	4.81	6.60	5.47	7.46	5.89	5.26	7.28	6.43	7.65
Ta	0.55	0.23	0.30	0.56	0.51	0.63	0.44	0.56	0.47	0.64	0.50	0.46	0.65	0.44	0.42
Zr	236	141	176	221	195	249	135	188	143	184	132	162	195	239	253
Th	8.83	3.26	3.97	8.00	6.17	8.62	5.04	5.69	4.73	6.54	4.82	5.12	6.79	10.26	17.76
U	1.20	0.69	0.67	1.09	0.90	2.11	5.83	8.28	1.97	1.92	2.11	2.02	1.98	0.79	0.90
Pb	13	15	12	9	11	20	14	16	11	12	11	11	12	9	14
Cu	5.9	2.2	5.9	3.7	10.3	11.6	11.3	11.9	7.3	9.6	8.4	9.1	9.2	5.8	6.0
Zn	60	43	58	66	54	65	67	79	68	66	59	55	66	133	107
Sc	8.50	5.87	6.15	8.52	7.41	7.24	6.07	6.64	5.81	7.33	5.65	5.22	7.18	6.78	8.19
V	66	37	48	68	60	62	42	42	43	59	44	43	59	68	59
Cr	70	70	57	67	60	71	77	77	52	83	75	65	49	64	63
Co	6	6	5	6	5	8	6	6	7	9	7	6	8	5	7
Ni	10.3	9.0	9.5	10.4	14.0	14.0	12.4	10.0	12.4	15.1	13.2	11.6	12.3	9.8	10.9

(*continued on next page*)

Table 1 (*continued*)

Component	K-9-3	K-9-4	K-1-4	K-1-8	K-10	K-10-1	K-10-2	K-10-3	K-10-4	K-10-5	K-11	2310270	GR-5	GR-6	K-9-2
	16	17	18	19	20	21	22	23	24	25	26	27	28	29	30
SiO_2	71.58	74.37	65.85	70.40	70.22	74.69	69.03	67.44	75.26	69.93	72.83	72.33	65.26	67.13	72.52
TiO_2	0.41	0.51	0.82	0.57	0.67	0.32	0.84	0.62	0.41	0.59	0.48	0.41	0.7	0.66	0.51
Al_2O_3	12.67	11.77	13.62	12.50	13.22	13.06	13.45	13.41	12.32	12.09	12.22	12.95	13.58	13.63	13.04
Fe_2O_3*	4.59	3.49	6.20	4.61	4.44	1.70	4.64	3.11	2.67	3.76	3.99	3.33	5.34	4.82	2.99
MnO	0.06	0.06	0.10	0.08	0.05	0.03	0.07	0.04	0.05	0.10	0.05	0.06	0.09	0.07	0.04
MgO	1.06	0.96	2.57	1.76	2.15	0.50	2.15	1.28	0.79	1.01	1.10	0.94	2.28	2.07	1.09
CaO	1.63	2.28	2.10	1.51	1.47	1.25	1.96	1.28	1.45	4.30	2.42	0.79	2.7	2.02	1.47
Na_2O	3.52	3.44	2.64	3.66	3.66	4.04	3.23	0.91	3.63	3.63	4.05	4.73	4.14	3.97	4.22
K_2O	3.22	1.98	2.89	2.11	3.12	3.49	3.31	4.27	2.72	2.45	1.71	2.48	2.37	2.60	3.15
P_2O_5	0.15	0.12	0.19	0.13	0.20	0.10	0.27	0.11	0.09	0.14	0.20	0.09	0.19	0.18	0.12
LOI	0.87	0.64	2.89	2.53	0.76	0.77	0.90	7.45	0.58	1.92	0.92	1.38	2.1	1.8	0.49
Total	99.76	99.62	99.87	99.86	99.96	99.95	99.85	99.92	99.97	99.92	99.97	99.49	98.75	98.95	99.64
Li	20.1	22.1	37.0	18.6	25.5	8.5	28.5	18.8	16.6	20.3	16.1	12.7	20.5	19.9	21.7
Ga	18.6	17.2	19.8	15.0	21.7	14.4	21.5	18.9	18.0	16.2	17.0	15.0	16.3	16.1	18.6
Rb	73	61	111	58	87	70	95	144	86	75	65	62	62	68	87
Sr	354	412	332	457	536	557	393	429	535	454	406	307	316	343	382
Ba	1682	810	712	694	1203	1648	1331	629	743	808	562	798	602	680	1368
La	43.9	40.7	33.7	24.3	41.9	26.7	56.8	40.1	34.6	39.7	47.3	19.0	30.6	28.7	65.4
Ce	81.9	76.3	74.4	50.5	77.7	51.5	114.2	82.2	67.3	80.9	93.9	40.7	65.6	58.1	126.3
Pr	7.99	7.96	7.72	5.71	8.18	5.57	12.51	8.12	6.64	8.06	9.51	4.24	7.22	6.58	13.10
Nd	32.8	33.4	32.2	24.5	35.8	23.4	48.3	33.3	26.5	30.2	38.0	15.7	28.1	25.5	46.5
Sm	5.33	4.90	6.02	4.37	5.96	3.71	7.96	5.68	4.61	4.80	6.03	2.70	5.21	4.78	6.47
Eu	1.17	0.96	1.23	0.90	1.36	0.68	1.57	0.99	0.75	1.08	1.28	0.69	1.24	1.19	1.31
Gd	4.98	3.85	6.95	4.24	4.99	3.05	7.59	5.38	4.31	5.34	5.95	2.80	5.61	5.07	6.39
Tb	0.46	0.37	0.83	0.55	0.48	0.33	0.71	0.53	0.45	0.58	0.57	0.34	0.70	0.63	0.55
Dy	2.64	2.22	4.83	3.48	2.86	2.06	3.55	3.07	2.59	2.73	2.83	1.80	3.79	3.49	2.67
Ho	0.45	0.34	0.83	0.57	0.44	0.31	0.54	0.50	0.44	0.50	0.50	0.34	0.71	0.65	0.42
Er	1.24	0.92	2.80	1.58	1.16	0.84	1.52	1.58	1.29	1.64	1.53	1.04	2.10	1.94	1.28
Tm	0.14	0.11	0.36	0.22	0.13	0.11	0.18	0.18	0.16	0.21	0.18	0.14	0.28	0.25	0.16
Yb	0.94	0.82	2.57	1.58	0.86	0.81	1.16	1.21	1.12	1.43	1.17	0.93	1.83	1.63	1.04
Lu	0.13	0.12	0.31	0.22	0.12	0.11	0.15	0.15	0.16	0.17	0.15	0.13	0.26	0.23	0.14
Y	11.0	8.4	23.2	15.4	11.0	8.2	13.5	11.9	11.3	12.0	12.2	8.7	18.0	16.3	10.1
Nb	5.32	5.34	10.63	4.96	7.13	4.07	9.19	6.41	7.62	9.01	7.07	3.97	7.73	6.97	7.64
Ta	0.33	0.35	0.65	0.35	0.44	0.31	0.54	0.38	0.63	0.57	0.39	0.31	0.63	0.51	0.45
Zr	223	192	199	244	223	199	299	274	247	220	231	149	255	190	240
Th	10.15	7.56	8.00	5.99	7.01	5.78	10.31	11.69	13.02	8.64	8.14	5.31	7.71	6.34	11.07
U	0.76	0.74	1.87	1.19	0.95	1.03	1.25	1.83	1.90	1.53	0.98	0.83	1.77	1.35	0.81
Pb	16	16	18	11	16	16	21	28	18	12	15	13	13	13	13
Cu	24.7	22.2	58.7	15.9	23.9	26.3	42.4	22.9	7.3	21.5	37.8	15.9	22.6	18.9	21.0
Zn	179	255	123	37	235	206	261	67	53	84	87	96	108	101	182
Sc	5.41	5.57	12.72	8.52	8.05	3.85	9.79	6.84	4.90	8.04	7.65	5.89	8.98	8.34	6.23
V	50	42	108	69	79	34	85	66	43	66	55	44	72	62	49
Cr	84	58	60	51	57	59	74	55	71	95	57	84	82	83	69
Co	5	6	15	7	9	4	13	3	5	11	6	8	9	7	6
Ni	8.8	11.1	30.4	18.1	17.5	8.4	26.0	12.5	9.6	28.8	13.0	20.1	19.1	17.6	11.7

Note. The contents of major components are in wt.%, and those of trace elements are in ppm. Fe_2O_3*, total iron as Fe_2O_3. 1–5, sandstones of the Malaya Tynda Formation of the Malaya Tynda depression; 6–29, sandstones of the Upper Dolokhit Subformation of the Strelka depression; 30, cement of conglomerates of the Upper Dolokhit Subformation.

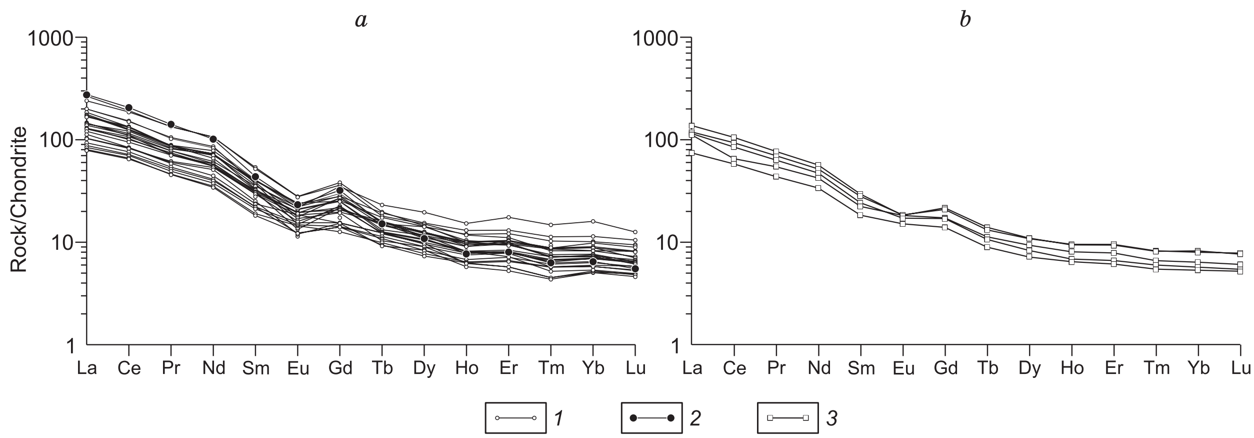

Fig. 3. Chondrite-normalized (McDonough and Sun, 1995) REE patterns of metasedimentary rocks of the Strelka (*a*) and Malaya Tynda (*b*) depressions. *1*, sandstones of the Upper Dolokhit Subformation of the Strelka depression; *2*, cement of conglomerates of the Upper Dolokhit Subformation; *3*, sandstones of the Malaya Tynda Formation of the Malaya Tynda depression.

of the above-mentioned compositional variations, several composition points (including the cement of the conglomerates) are shifted into the field of arkoses, and the other rocks are similar in composition to schists (Fig. 2*b*).

The REE patterns of sandstones and the cement of conglomerates of the Upper Dolokhit Subformation (Fig. 3*a*) clearly show domination of LREE over HREE ($[La/Yb]_n$ = 10.4–38.0) and a moderate negative Eu anomaly (Eu/Eu* = 0.50–0.92). The contents of most of lithophile elements in the studied rocks (Fig. 4*a*) are close to the upper-crust ones, except for a slight deficit of U, Nb, Ta, Y, HREE, and, in some samples, Zr and higher contents of V and Cr.

Sandstones of the Malaya Tynda Formation of the Malaya Tynda depression are gray to dark gray medium-grained rocks with a psammitic texture and a massive or, less often, schistose structure. The nongraded clastic material 0.1–

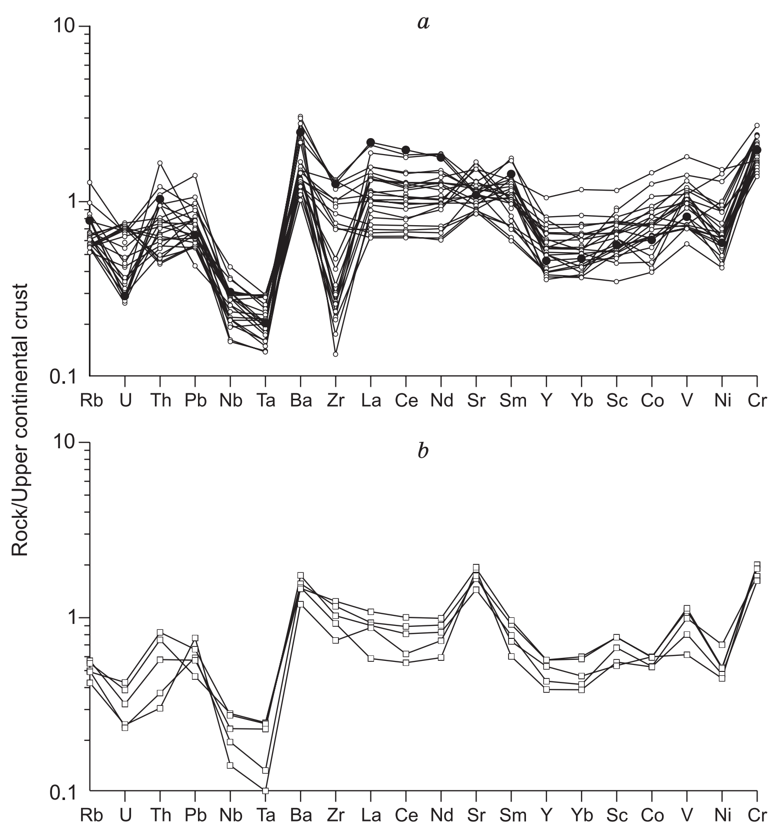

Fig. 4. Upper continental crust-normalized (Taylor and McLennan, 1985) trace-element patterns of metasedimentary rocks of the Strelka (*a*) and Malaya Tynda (*b*) depressions. Designations follow Fig. 3.

0.8 mm in size consists mostly of semiangular grains of quartz (55–65%) and feldspars (30–35%). There are also fragments of microquartzites and schists (up to 10%). The accessory minerals are zircon, garnet, and magnetite. The rock cement is of contact, contact–pore, and basalt types.

In the proportions of rock-forming components sandstones of the Malaya Tynda Formation correspond to graywackes (Fig. 2*a*) or wackes (Fig. 2*b*). Like the least silicic rocks of the Upper Dolokhit Subformation, they are close in composition to schists (Fig. 2*b*). The trace-element patterns of these sandstones (Figs. 3*b* and 4*b*) and metasedimentary rocks of the Strelka depression (Figs. 3*a* and 4*a*) are similar.

RESULTS OF U–Th–Pb GEOCHRONOLOGICAL STUDY

A U–Th–Pb geochronological study was carried out for detrital zircons from sandstone (sample R-25) and the cement of medium-pebble conglomerate (sample K-9-2) of the Upper Dolokhit Subformation of the Strelka depression and for sandstone (sample R-19) of the Malaya Tynda Formation of the Malaya Tynda depression. The results of study are given in Fig. 5; the sampling localities are shown in Fig. 1.

A concordant age was determined for 113 of 127 studied grains of detrital zircons from sandstone of the Upper Dolokhit Subformation. This age is mostly within 156–211 and 341–368 Ma. The peaks in the relative-probability curve correspond to ages of 164, 196, and 358 Ma (Fig. 5*a*). There are also few zircon grains with a concordant age of 222, 397, and 871 Ma.

A concordant age was determined for 72 of 115 studied grains of detrital zircons from the cement of the medium-pebble conglomerate of the Upper Dolokhit Subformation. It is within 162–213, 339–357, 1862–2031, 2160–2260, and 2381–2591 Ma. The peaks in the relative-probability curve correspond to ages of 170, 179, 349, 1890, 2018, 2438, and 2520 Ma (Fig. 5*b*).

A concordant age was determined for 82 of studied 127 grains of detrital zircons from sandstone of the Malaya Tynda Formation. It is within 162–194, 223–233, 331–347, 1770–1998, and 2480–2648 Ma. The clearest peaks in the relative-probability curve correspond to ages of 171, 230, 343, and 1873 Ma (Fig. 5*c*).

RESULTS OF Lu–Hf ISOTOPE-GEOCHEMICAL STUDY

A Lu–Hf isotope-geochemical study was carried out at the same sites of zircons as the U–Th–Pb study. We analyzed 20–25 grains of each zircon sample, choosing sites with concordant ages. The results are presented in Table 2 and in Fig. 6.

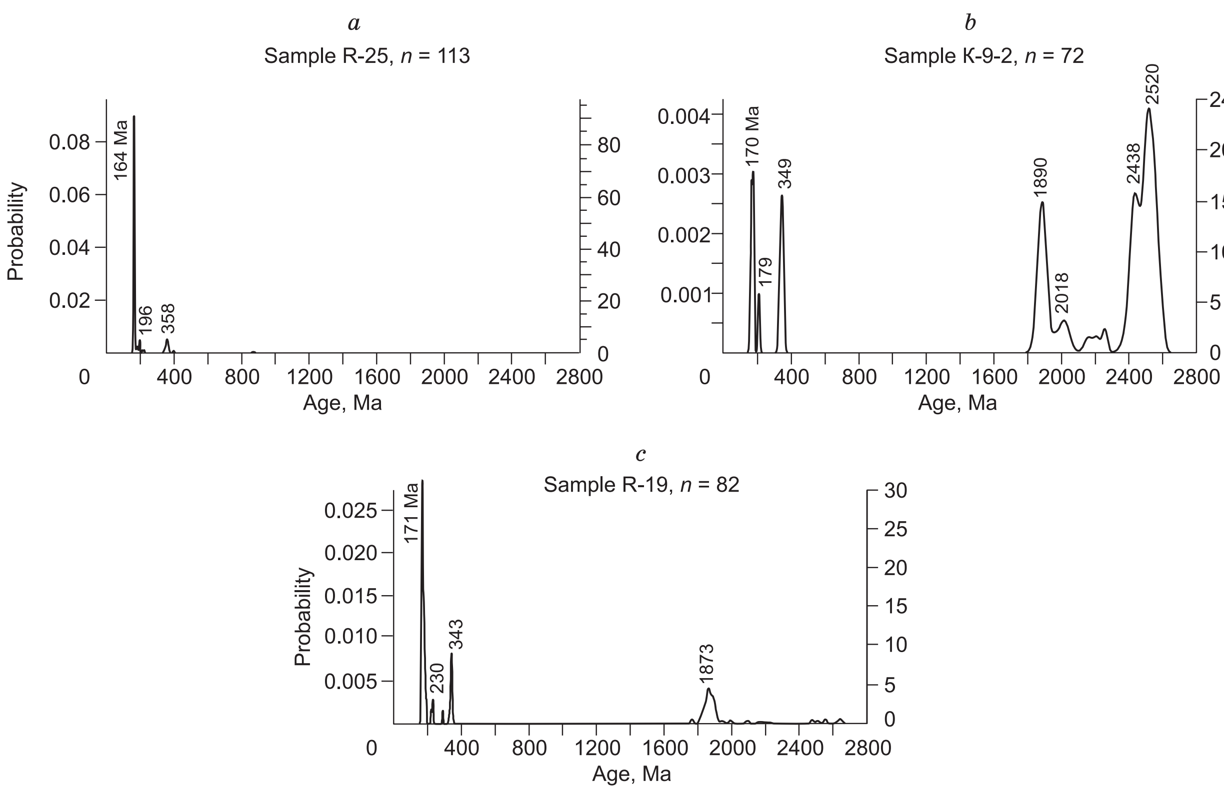

Fig. 5. Relative-probability–age curves for detrital zircons from sandstone of the Upper Dolokhit Subformation of the Strelka depression (sample R-25) (*a*), from the cement of conglomerate of the Upper Dolokhit Subformation (sample K-9-2) (*b*), and from sandstone of the Malaya Tynda Formation of the Malaya Tynda depression (sample R-19) (*c*). *n*, number of concordant-age estimates used for the curve construction.

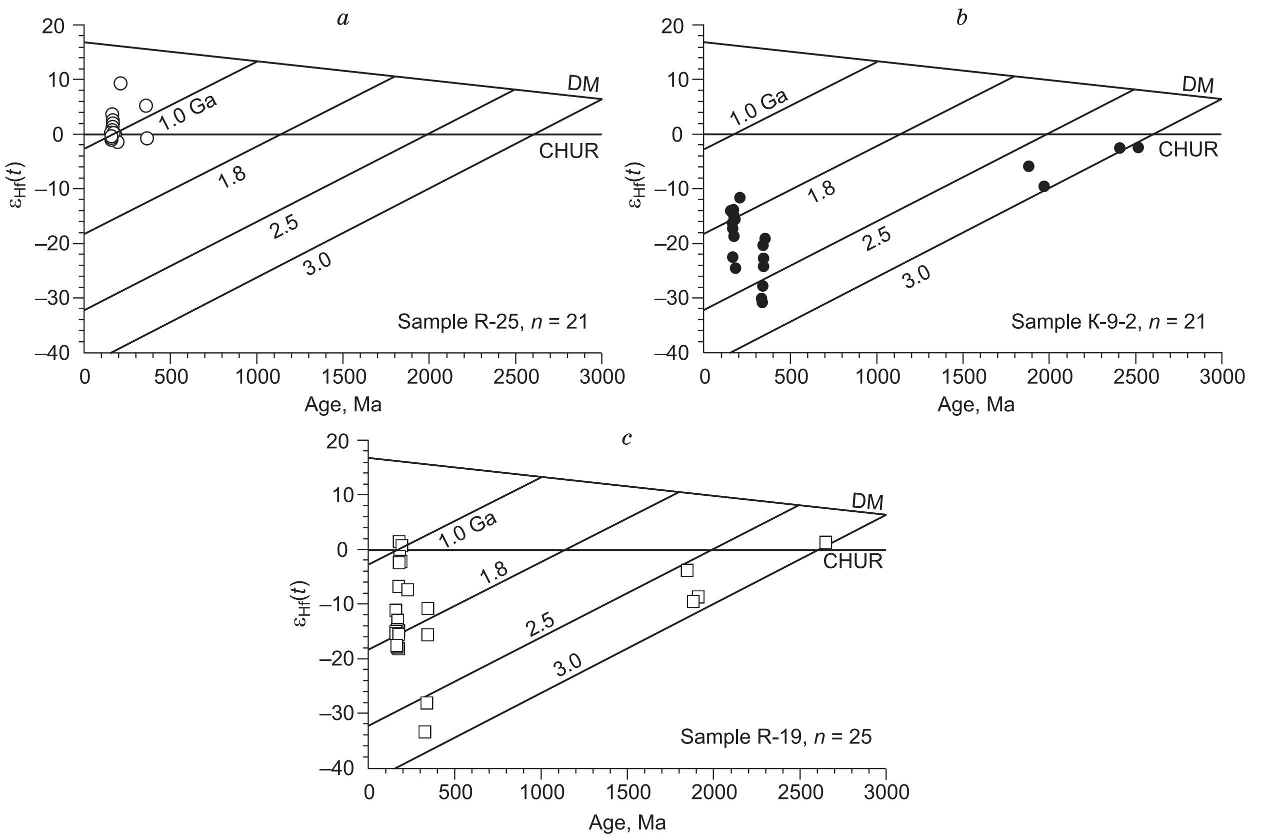

Fig. 6. $\varepsilon_{Hf}(t)$–age (Ma) diagram for zircons from sandstone of the Upper Dolokhit Subformation of the Strelka depression (sample R-25) (*a*), from the cement of conglomerate of the Upper Dolokhit Subformation (sample K-9-2) (*b*), and from sandstone of the Malaya Tynda Formation of the Malaya Tynda depression (sample R-19) (*c*). *n*, number of measurements made for the plot construction. DM, depleted mantle, CHUR, chondritic uniform reservoir.

As seen from the above data, zircons from sandstone of the Upper Dolokhit Subformation (sample R-25) are characterized by positive and weakly negative (close to zero) $\varepsilon_{Hf}(t)$ values, from +9.3 to –1.3, and model ages $t_{Hf}(C)$ of 0.6–1.2 Ga (Fig. 6*a*, Table 2).

Zircons from the cement of medium-pebble conglomerate (sample K-9-2) of the same subformation show, on the contrary, negative $\varepsilon_{Hf}(t)$ values, from –2.4 to –30.7, and older model ages $t_{Hf}(C)$, 1.6–3.0 Ga (Fig. 6*b*, Table 2).

The most intricate pattern is observed for the Hf isotope composition of zircons from sandstone of the Malaya Tynda Formation (sample R-19) (Fig. 6*c*, Table 2), which is due to the wide variations in isotope parameters. For example, there is a small group of zircons with an age of 181 to 194 Ma, $\varepsilon_{Hf}(t)$ of +1.6 to –2.0, and $t_{Hf}(C)$ = 0.9–1.1 Ga. The rest zircons, independently of their crystallization age, are characterized by a significantly older model age, t_{Hf}(C) = 1.4–2.9 Ga (Fig. 6*c*, Table 2).

THE AGE OF SEDIMENTARY COMPLEXES AND THE SOURCES OF CLASTIC MATERIAL

The U–Th–Pb geochronological study has shown that the youngest zircons in both sandstones (sample R-25) and conglomerates (sample K-9-2) of the Upper Dolokhit Subformation of the Strelka depression are of Upper Jurassic age, which contradicts its stratigraphic Middle Jurassic age (Petruk and Kozlov, 2009; Koshelenko, 2011) determined on the basis of fossil fauna. This is probably because fauna description was made for the Lower Dolokhit Subformation only, whereas the geochronological study was carried out for zircons from rocks of the Upper Dolokhit Subformation, which might be younger.

Note that zircons from two samples of metasedimentary rocks of the Upper Dolokhit Subformation of the Strelka depression (R-25 and K-9-2) show significantly different curves of the relative age probability.

For example, early Precambrian zircons are strongly predominant in the cement of conglomerates (sample K-9-2) (Fig. 5*b*). Taking into account the structure of the study region, we regard early Precambrian complexes on the southern framing of the North Asian Craton as the most likely source of these zircons. We believe that the most ancient zircons were supplied into the Strelka depression as a result of the destruction of Neoarchean rocks of the Stanovoi complex, whose protoliths are dated at 2.6–2.9 Ga (Velikoslavinskii et al., 2011, 2017), and of Neoarchean and Paleoproterozoic intrusions (Buchko et al., 2006, 2008;

Table 2. Results of Lu–Hf isotope study of zircons from metasedimentary rocks of the Strelka and Malaya Tynda depressions

No.	Sample/ Grain no.	Age, Ma	$(^{176}Yb+^{176}Lu)/^{176}Hf$ (%)	$^{176}Lu/^{177}Hf$	$^{176}Hf/^{177}Hf$	$\varepsilon_{Hf}(t)$	t_{Hf}(DM)	t_{Hf}(C)
Sandstones of the Upper Dolokhit Subformation of the Strelka depression								
1	R-25/89	156	5.6	0.000335	0.282677 ± 27	0.03	0.80	1.0
2	R-25/56	160	7.0	0.000427	0.282687 ± 25	0.5	0.79	1.0
3	R-25/78	161	6.7	0.000385	0.282648 ± 21	–0.9	0.84	1.0
4	R-25/111	161	8.1	0.000498	0.282776 ± 25	3.6	0.67	0.8
5	R-25/74	162	5.6	0.000339	0.282684 ± 21	0.4	0.79	1.0
6	R-25/44	162	6.3	0.000385	0.282671 ± 21	–0.1	0.81	1.0
7	R-25/96	163	5.2	0.000311	0.282676 ± 26	0.2	0.80	1.0
9	R-25/114	163	10.7	0.000662	0.282686 ± 23	0.5	0.79	1.0
10	R-25/85	163	7.3	0.000445	0.282701 ± 20	1.0	0.77	0.9
11	R-25/12	164	6.6	0.000400	0.282711 ± 23	1.4	0.75	0.9
12	R-25/53	164	7.8	0.000471	0.282688 ± 26	0.6	0.79	1.0
13	R-25/124	165	7.8	0.000475	0.282728 ± 27	2.0	0.73	0.9
14	R-25/29	165	6.5	0.000396	0.282642 ± 27	–1.0	0.85	1.1
15	R-25/28	166	6.1	0.000387	0.282741 ± 26	2.5	0.71	0.9
16	R-25/61	167	8.7	0.000523	0.282649 ± 22	–0.7	0.84	1.0
17	R-25/93	178	10.4	0.000648	0.282662 ± 22	–0.1	0.83	1.0
18	R-25/18	194	17.0	0.001303	0.282620 ± 22	–1.3	0.90	1.1
19	R-25/91	211	29.4	0.001695	0.282910 ± 33	9.3	0.49	0.6
20	R-25/98	357	29.3	0.001783	0.282710 ± 21	5.3	0.78	0.9
21	R-25/107	366	20.1	0.001257	0.282531 ± 30	–0.8	1.03	1.2
Conglomerates of the Upper Dolokhit Subformation of the Strelka depression								
22	K-9-2/68	162	9.7	0.000508	0.282272 ± 14	–14.2	1.36	1.7
23	K-9-2/39	169	12.2	0.000714	0.282031 ± 18	–22.6	1.71	2.1
24	K-9-2/47	177	20.5	0.001305	0.282272 ± 18	–14.0	1.39	1.7
25	K-9-2/11	186	22.0	0.001570	0.281961 ± 31	–24.8	1.84	2.3
26	K-9-2/1	213	25.8	0.001410	0.282314 ± 21	–11.7	1.34	1.6
27	K-9-2/6	341	6.5	0.000434	0.281696 ± 15	–30.7	2.15	2.7
28	K-9-2/93	345	10.0	0.000656	0.281778 ± 18	–27.7	2.05	2.5
29	K-9-2/118	353	8.9	0.000542	0.281914 ± 16	–22.7	1.86	2.3
30	K-9-2/8	168	15.9	0.000927	0.282181 ± 18	–17.3	1.51	1.9
31	K-9-2/10	174	6.8	0.000394	0.282201 ± 15	–16.4	1.46	1.8
32	K-9-2/105	175	16.7	0.000940	0.282242 ± 21	–15.0	1.42	1.8
33	K-9-2/70	180	9.9	0.000593	0.282131 ± 16	–18.8	1.56	2.0
34	K-9-2/122	181	8.3	0.000495	0.282217 ± 14	–15.7	1.44	1.8
35	K-9-2/124	335	10.0	0.000647	0.281713 ± 15	–30.2	2.14	2.7
36	K-9-2/29	345	18.8	0.001257	0.281987 ± 20	–20.5	1.79	2.2
37	K-9-2/101	350	10.8	0.000647	0.281871 ± 19	–24.3	1.92	2.4
38	K-9-2/104	357	10.4	0.000685	0.282009 ± 14	–19.3	1.73	2.1
39	K-9-2/120	1887	4.7	0.000251	0.281420 ± 17	–6.1	2.51	2.7
40	K-9-2/7	1976	8.2	0.000511	0.281269 ± 17	–9.8	2.73	2.9
41	K-9-2/13	2409	8.2	0.000495	0.281192 ± 16	–2.7	2.83	2.9
42	K-9-2/30	2519	8.3	0.000489	0.281128 ± 13	–2.4	2.92	3.0
Sandstones of the Malaya Tynda Formation of the Malaya Tynda depression								
43	R-19/41	161	9.9	0.000578	0.282362 ± 16	–11.0	1.24	1.6
44	R-19/102	166	10.9	0.000651	0.282238 ± 19	–15.3	1.42	1.8
45	R-19/117	168	15.9	0.001065	0.282253 ± 17	–14.8	1.41	1.8
46	R-19/24	169	8.7	0.000569	0.282257 ± 14	–14.6	1.39	1.7

(*continued on next page*)

Table 2 (*continued*)

No.	Sample/ Grain no.	Age, Ma	(^{176}Yb+^{176}Lu)/ ^{176}Hf (%)	^{176}Lu/^{177}Hf	^{176}Hf/^{177}Hf	$\varepsilon_{Hf}(t)$	t_{Hf}(DM)	t_{Hf}(C)
47	R-19/90	170	8.5	0.000551	0.282164 ± 18	–17.8	1.52	1.9
48	R-19/6	171	9.5	0.000568	0.282235 ± 24	–15.3	1.42	1.8
49	R-19/93	171	10.6	0.000632	0.282303 ± 18	–12.9	1.33	1.7
50	R-19/77	174	17.3	0.001031	0.282235 ± 21	–15.3	1.44	1.8
51	R-19/92	175	15.2	0.000945	0.282156 ± 17	–18.0	1.54	1.9
52	R-19/59	177	9.1	0.000558	0.282245 ± 15	–14.8	1.40	1.8
53	R-19/66	179	11.0	0.000717	0.282476 ± 21	–6.6	1.09	1.4
54	R-19/1	181	12.1	0.000770	0.282608 ± 15	–1.9	0.91	1.1
55	R-19/76	182	12.6	0.000872	0.282624 ± 18	–1.3	0.89	1.1
56	R-19/4	183	9.8	0.000599	0.282706 ± 18	1.6	0.76	0.9
57	R-19/83	190	16.1	0.000945	0.282602 ± 17	–2.0	0.92	1.1
58	R-19/74	194	25.2	0.001731	0.282681 ± 22	0.8	0.82	1.0
59	R-19/72	231	19.7	0.001181	0.282426 ± 19	–7.3	1.17	1.4
60	R-19/40	330	12.8	0.000767	0.281627 ± 21	–33.4	2.26	2.8
61	R-19/121	342	7.5	0.000496	0.281769 ± 15	–28.1	2.05	2.6
62	R-19/22	345	6.7	0.000450	0.282120 ± 15	–15.6	1.57	1.9
63	R-19/68	346	51.9	0.003318	0.282276 ± 22	–10.7	1.47	1.7
64	R-19/120	1845	15.5	0.000958	0.281538 ± 19	–3.7	2.39	2.5
65	R-19/96	1877	5.9	0.000337	0.281335 ± 17	–9.4	2.63	2.8
66	R-19/44	1910	7.0	0.000409	0.281340 ± 20	–8.6	2.63	2.8
67	R-19/103	2646	4.1	0.000236	0.281145 ± 16	1.5	2.88	2.9

Note. The errors (1σ) of ^{176}Hf/^{177}Hf determination correspond to the last significant figures.

Velikoslavinskii et al., 2017), which underwent structure-metamorphic transformations at 2.6 and 1.9 Ga (Velikoslavinskii et al., 2012a,b, 2017). Granitoids of the Olekma complex (358 ± 2 Ma (Larin et al., 2015); 360 ± 2 Ma (Velikoslavinskii et al., 2016a)) and volcanics of the Amazar–Gilyui zone (358 ± 2 Ma (Velikoslavinskii et al., 2016a)) can be regarded as the sources of Carboniferous zircons (~349 Ma) (Fig. 5*b*).

As seen from the relative age probability curves (Fig. 5*b*), the youngest ages of zircons from the cement of conglomerates of the Upper Dolokhit Subformation are 170 and 179 Ma. The most likely sources of these zircons are granitoids of the Tok–Algoma igneous complex of the Selenga–Stanovoi superterrane, dated at 177 ± 3 and 173 ± 1 Ma (Kotov et al., 2012). A close age (178 ± 2 and 177 ± 2 (Sorokin et al., 2015a)) was established for volcanics in the southwest of the Dzhugdzhur–Stanovoi superterrane and for metavolcanics (193 ± 1 Ma (Velikoslavinskii et al., 2012a)) of the Amazar–Gilyui zone of the Selenga–Stanovoi superterrane.

Recall that all zircons from the studied conglomerates have ancient model ages $t_{Hf}(C)$ = 1.6–3.0 Ga (Fig. 6*b*, Table 2).

Thus, the results obtained show that igneous and metamorphic complexes on the southern framing of the North Asian Craton were the main source of material, including zircons found in the cement of conglomerates of the Upper Dolokhit Subformation. This model is confirmed by the predominance of metamorphic rocks in the clastic material of these conglomerates.

Sandstones (sample R-25) of the Upper Dolokhit Subformation of the Strelka depression are almost free of early Precambrian zircons (Fig. 5*a*). Therefore, clastic material could not have arrived from the southern framing of the North Asian Craton during its accumulation. The same is evidenced by the model ages of zircons, $t_{Hf}(C)$ = 0.6–1.2 Ga (Table 2).

Taking into account the location of the Strelka depression between the Mongol–Okhotsk Belt and the Selenga–Stanovoi superterrane (Fig. 1), we admit that this material was supplied from the Mongol–Okhotsk Belt. This interpretation is consistent with the presence of Carboniferous, Late Triassic, and Early Jurassic zircons in metasedimentary rocks of this belt (Sorokin et al., 2015b, 2017; Zaika et al., 2018, 2019; our unpublished data). In this case, however, the source of Middle Jurassic zircons (164 Ma) in sandstones of the Upper Dolokhit Subformation remains unclear. We will return to this problem below.

In sandstones (sample R-19) of the Malaya Tynda Formation of the Malaya Tynda depression, the age groups of zircons are close to those of zircons in conglomerates of the Strelka depression. For example, the relative age probability curve of zircons (Fig. 5*c*) have distinct peaks of 171, 230, 343, and 1873 Ma; in addition, there are many zircons with ages within 2480–2648 Ma. Taking into account the identical structural position of these depressions, we assume that the clastic material present in sandstones of the Malaya Tynda Formation was also supplied from igneous and metamorphic complexes of the southern framing of the North Asian Craton. Above, we described the probable sources of zircons with an age of ~171 Ma and with early Precambrian ages. As for zircons with ages of ~230 and ~343 Ma, they are nearly coeval with metarhyolites of the Gilyui metamorphic complex (231 ± 4 Ma (Velikoslavinskii et al., 2016b)) and diorites of the Tok–Algoma complex (238 ± 2 Ma (Sal'nikova et al., 2006). The hypothesis of the predominant drift of material into the Malaya Tynda depression agrees with the ancient model ages of most of clastic zircons, $t_{Hf}(C)$ = 1.4–2.9 Ga (Fig. 6*c*, Table 2). At the same time, sandstones of the Malaya Tynda Formation contain zircons dated at 181–194 Ma and having younger model ages $t_{Hf}(C)$ = 0.9–1.1 Ga (Fig. 6*c*, Table 2). This suggests that part of zircons and part of clastic material were supplied into the Malaya Tynda depression from other sources, e.g., the Mongol–Okhotsk Belt.

THE TECTONIC NATURE OF THE DEPRESSIONS

As mentioned above, the chemical compositions of rocks of the Strelka and Malaya Tynda depressions show significant variations (Fig. 2, Table 1). We think this is due to the wide variety of rocks in the sources of clastic material. Our hypothesis is supported by the Na_2O–CaO–K_2O (Fig. 7*a*)

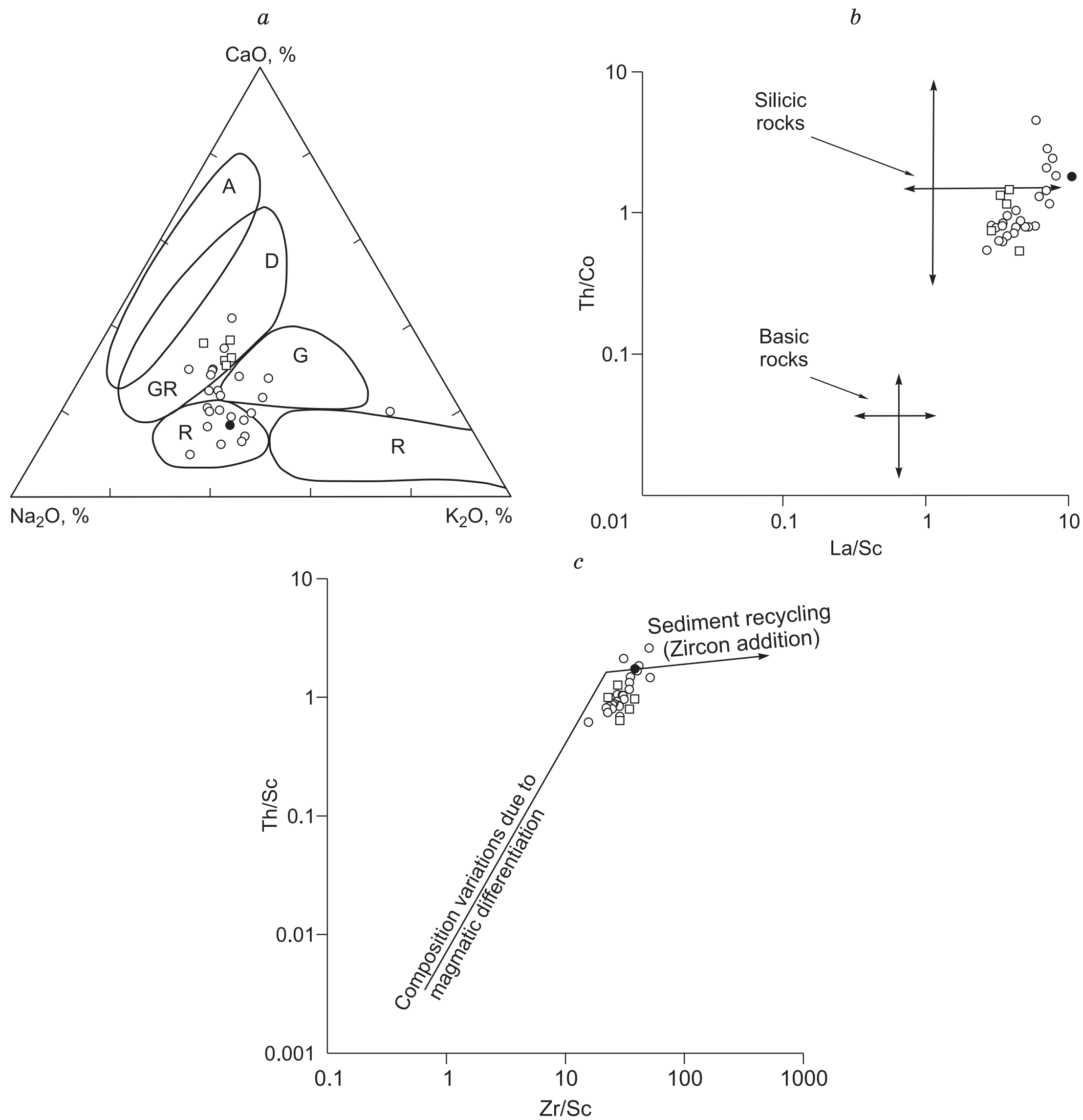

Fig. 7. Na_2O–CaO–K_2O (Bhatia, 1983) (*a*), La/Sc–Th/Co (Cullers, 2002) (*b*), and (Zr/Sc)–(Th/Sc) (McLennan, 1993) (*c*) diagrams for metasedimentary rocks of the Strelka and Malaya Tynda depressions. Fields: A, andesites; D, dacites; Gr, granodiorites; G, granites; R, recycled sediments. Fe_2O_3*, total iron as Fe_2O_3. Designations follow Fig. 2.

and La/Sc–Th/Co (Fig. 7*b*) diagrams demonstrating a predominance of both acid and moderately acid rocks in the provenances. Some rocks in the studied depressions, primarily siliceous sandstones and the cement of conglomerates of the Upper Dolokhit Subformation, correspond in composition to recycled sediments (Fig. 7*a*, *c*). Apparently, these rocks (sample K-9-2) received material from the southern framing of the North Asian Craton via intermediate collectors (e.g., sedimentary gneisses).

The above-noted chemical variations are also observed in tectonic diagrams. Independently of the chemical parameters used to construct the diagrams, the composition points of metasedimentary rocks of the Strelka and Malaya Tynda depressions overlap the composition fields of sediments formed in different geodynamic settings (Fig. 8*a*–*d*). For example, the rocks of the studied depressions are similar in the ($Fe_2O_3^*$+ MgO)–Al_2O_3/(CaO+Na_2O) and ($Fe_2O_3^*$+ MgO)–TiO_2 correlations to island-arc sediments of the continental basement and active continental margins. At the same time, part of the sandstone samples from the Upper Dolokhit Subformation is similar in composition to oceanic-arc sediments, and another part, to sediments of passive continental margins (Fig. 8*a*, *b*). Many rocks of the Strelka and Malaya Tynda depressions correspond in the La/Sc–Ti/Zr correlation to sediments of active continental margins (Fig. 8*c*). The F1–F2 diagram shows that the metasedimentary rocks of the studied depressions are compositionally similar to sedimentary rocks of subduction settings (Fig. 8*d*).

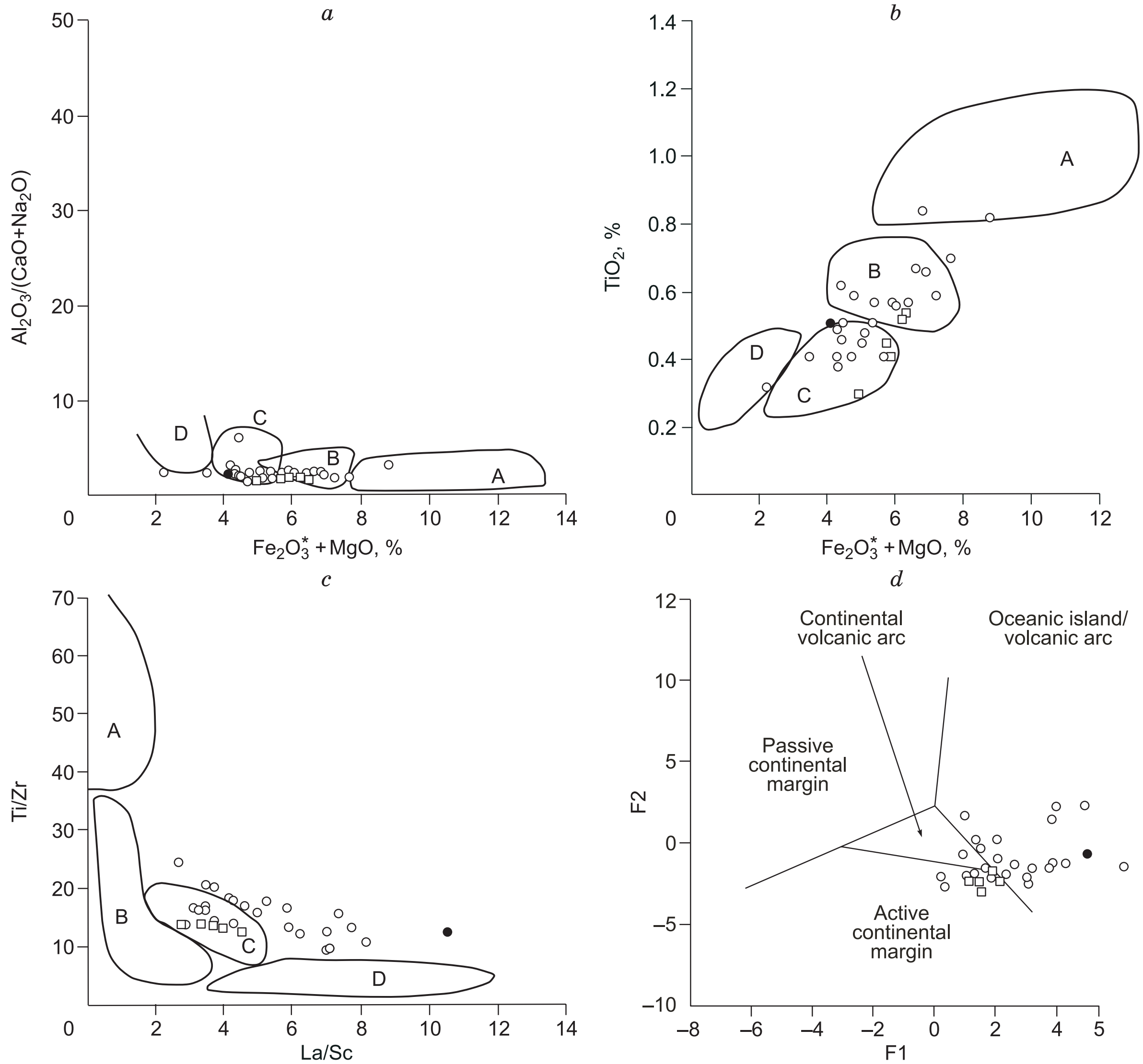

Fig. 8. Na_2O–CaO–K_2O (*a*) (Bhatia, 1983), La/Sc–Th/Co (Cullers, 2002) (*b*), ($Fe_2O_3^*$ + MgO)–Al_2O_3/(CaO + Na_2O) (Bhatia, 1983) (*c*), ($Fe_2O_3^*$ + MgO)–TiO_2 (Bhatia, 1983) (*d*), La/Sc–Ti/Zr (Bhatia, 1983) (*e*), and F1–F2 (Bhatia, 1983) (*f*) tectonic diagrams for metasedimentary rocks of the Strelka and Malaya Tynda depressions. Designations follow Fig. 2. Fields of sandstones from tectonic settings: A, oceanic island arcs; B, continental island arcs; C, active continental margins; D, passive continental margins. $Fe_2O_3^*$, total iron as Fe_2O_3. F1 = 0.303 – 0.0447SiO_2 – 0.972TiO_2 + 0.008Al_2O_3 – 0.267Fe_2O_3 + 0.208FeO – 0.082MnO + 0.14MgO + 0.195CaO + 0.719Na_2O – 0.032K_2O + 7.51P_2O_5; F2 = 43.57 – 0.421 SiO_2 – 1.988 TiO_2 + 0.526Al_2O_3 – 0.551Fe_2O_3 + 1.61FeO – 2.72MnO + 0.881MgO + 0.907CaO + 0.177Na_2O – 1.84K_2O + 7.244P_2O.

The above compositional features are specific to synorogenic sedimentary rocks (Maslov et al., 2013, 2015), which suggests the orogenic nature of the studied depressions.

In Introduction we mentioned that the Strelka and Malaya Tynda depressions join the Mongol–Okhotsk Orogenic Belt in the north and extend along the boundary between the belt and the southern framing of the North Asian Craton (Fig. 1). This structural position permits them to be considered marginal troughs. Both troughs are filled with thick beds of marine (at the bottom) and continental (at the top) terrigenous rocks, with an increase in the grain size of clastic material up the section. Therefore, the rocks should be regarded as molasse.

To elucidate the tectonic nature of the Strelka and Malaya Tynda depressions, it is necessary to consider their age correlation with the Mongol–Okhotsk Belt. The age of the fossil fauna indicates that the depressions formed and evolved from the early Middle Jurassic through the early Early Cretaceous. The youngest zircons in their rocks have a Late Jurassic age: 156 Ma (sample R-25), 162 Ma (sample K-9-2), and 162 Ma (sample R-19). The fossil fauna in the deposits of the Mongol–Okhotsk Belt poorly substantiates their age (Resolutions..., 1994; Khanchuk, 2006; Serezhnikov and Volkova, 2007; Petruk and Kozlov, 2009), but the available data indicate that the youngest paleo-oceanic sediments formed in the Early–Middle Jurassic (Parfenov et al., 1999).

The results of recent geochronological studies show that the single youngest zircons in metasediments of the Yankan (Sorokin et al., 2015b), Tukuringra (Sorokin et al., 2017; Zaika et al., 2018), and Un'ya–Bom (Zaika et al., 2019) terranes of the Mongol–Okhotsk Belt are of Early Jurassic age, ~175 Ma. Note that the youngest zircons (164, 170, and 171 Ma) prevailing in sedimentary rocks of the Strelka and Malaya Tynda depressions are absent from deposits of the Mongol–Okhotsk Belt. This indicates that both depressions originated after the complete closure of the Mongol–Okhotsk basin and the formation of an orogenic structure at its place. It is also evident that orogenic processes in the east of the Mongol–Okhotsk Belt were completed at the Early–Middle Jurassic boundary. A similar tectonic model was earlier proposed for the western part of the belt (Demonterova et al., 2017).

The above facts confirm our hypothesis that the clastic material filling the Strelka and Malaya Tynda depressions was supplied from both the southern framing of the North Asian Craton and the Mongol–Okhotsk Orogenic Belt. Moreover, they explain the presence of zircons of Middle–Late Jurassic boundary age (164 Ma) and young model age t_{Hf}(C) = 0.8–1.0 Ga (Table 2) in sandstones (sample R-25) of the Strelka depression. Accepting that orogenic processes in the east of the Mongol–Okhotsk Belt were completed in the late Early Jurassic and that the belt-framing continental structures (the Amur superterrane in the south and the North Asian Craton in the north) became proximal to each other, we admit that the youngest zircons (164 Ma) got into the Strelka depression from the Amur superterrane. This hypothesis is supported by the presence of igneous complexes with the similar ages and isotope-geochemical parameters (t_{Hf}(C)) of zircons in the north of the superterrane (Gou et al., 2013; Tang et al., 2015).

Thus, the results obtained indicate that orogenic processes in the east of the Mongol–Okhotsk Belt were completed at the Early–Middle Jurassic boundary. On the other hand, according to the available paleomagnetic data (Zhao et al., 1994; Halim et al., 1998; Kravchinsky et al., 2002; Metelkin et al., 2004, 2007, 2010; Ren et al., 2016), the North Asian and North China Cratons and some tectonic blocks in Mongolia and Transbaikalia had different paleopositions till the Early Cretaceous. We think that this difference was the result of intense intraplate shear displacements caused by the rotation of the North Asian Craton relative to the Southeast Asian and East Asian continental massifs in the late Mesozoic. In particular, sinistral intraplate displacements took place throughout the Mesozoic. The paleomagnetic data (Halim et al., 1998; Metelkin et al., 2004, 2007) reveal them from the Triassic to the Cretaceous. These displacements are evidenced by the presence of tectonic bodies of early Paleozoic granitoids among Permian(?) (or younger) rocks in the axial zone of the Mongol–Okhotsk Belt (Sorokin et al., 2007).

CONCLUSIONS

Based on the results obtained, we can draw the following conclusions:

(1) The Strelka and Malaya Tynda depressions bordering the Mongol–Okhotsk Orogenic Belt in the north and extending along the boundary between the belt and the southern framing of the North Asian Craton are marginal troughs. They are filled with thick beds of Mesozoic marine (at the bottom) and continental (at the top) terrigenous rocks, with an increase in the grain size of clastic material up the section; the rocks should be regarded as molasses.

(2) The results of U–Th–Pb geochronological study of detrital zircons from metasediments of the Strelka and Malaya Tynda depressions and the eastern Mongol–Okhotsk Orogenic Belt show that orogenic processes in this part of the belt were completed at the Early–Middle Jurassic boundary. The above depressions began to form after the complete closure of the Mongol–Okhotsk Basin and the formation of an orogenic structure at its place.

(3) The depressions were filled with material supplied both from the Selenga–Stanovoi and Dzhugdzhur–Stanovoi superterranes on the southern framing of the North Asian Craton and from the Mongol–Okhotsk Belt, which was a mountain-folded structure in the Middle Jurassic.

(4) After the completion of collision processes, the folded structures of the Mongol–Okhotsk Belt transformed as a result of intense shear displacements in the Late Mesozoic.

We thank the analysts from the Institute of Geology and Nature Management (E.N. Voropaev, O.G. Medvedev, A.I. Palazhchenko, V.I. Rozhdestvin, E.S. Sapozhnik, and

E.V. Ushakov), Yu.A. Kosygin Institute of Tectonics and Geophysics, Khabarovsk (E.M. Golubev, A.V. Shtarev, and L.S. Bokovenko), and the Arizona LaserChron Center, USA, for the sample analyses. We are sincerely grateful to T.V. Donskaya for the careful review of the manuscript, discussion, and constructive remarks.

The mineralogical investigations were carried out in accordance with the research project AAAA-A16-116051810110-7 of the Institute of Geology and Nature Management, and the geochemical, isotope-geochemical, and geochronological studies were supported by grant 18-35-00002 from the Russian Foundation for Basic Research.

REFERENCES

Amelin, Y., Lee, D.-C., Halliday, A.N., Pidgeon, R.T., 1999. Nature of the Earth's earliest crust from hafnium isotopes in single detrital zircons. Nature 399, 252–255.

Bhatia, M.R., 1983. Plate tectonics and geochemical composition of sandstones. J. Geol 91 (6), 611–627.

Black, L.P., Kamo, S.L., Allen, C.M., Davis, D.W., Aleinikoff, J.N., Valley, J.W., Mundil, R., Campbell, I.H., Korsch, R.J., Williams, I.S., Foudoulis, C., 2004. Improved $^{206}Pb/^{238}U$ microprobe geochronology by the monitoring of trace-element-related matrix effect; SHRIMP, ID-TIMS, ELA-ICP-MS and oxygen isotope documentation for a series of zircon standards. Chem. Geol. 205, 15–140.

Blichert-Toft, J., Albarede, F., 1997. The Lu–Hf geochemistry of chondrites and the evolution of the mantle–crust system. Earth Planet. Sci. Lett. 148, 243–258.

Buchko, I.V., Sal'nikova, E.B., Kotov, A.B., Larin, A.M., Velikoslavinskii, S.D., Sorokin, A.A., Sorokin, A.P., Yakovleva, S.Z., 2006. Paleoproterozoic gabbroanorthosites of the Selenga–Stanovoi superterrane, southern framing of the Siberian Craton. Dokl. Earth Sci. 407A (3), 372–375.

Buchko, I.V., Sorokin, A.A., Sal'nikova, E.B., Kotov, A.B., Larin, A.M., Sorokin, A.P., Velikoslavinskii, S.D., Yakovleva, S.Z., 2008. Age and tectonic setting of the Kengurak–Sergachi gabbro-anorthosite massif (the Selenga–Stanovoi superterrane, southern frame of the Siberian craton). Stratigr. Geol. Correl. 16 (4), 349–359.

Buchko, I.V., Sorokin, A.A., Sal'nikova, E.B., Kotov, A.B., Velikoslavinskii, S.D., Larin, A.M., Izokh, A.E., Yakovleva, S.Z., 2010. The Triassic stage of mafic magmatism in the Dzhugdzhur–Stanovoi superterrane (southern framing of the North Asian craton). Russian Geology and Geophysics (Geologiya i Geofizika) 51 (11), 1157–1166 (1489–1500).

Buchko, I.V., Sorokin, A.A., Kotov, A.B., Samsonov, A.V., Larionova, Yu.A., Ponomarchuk, A.V., Larin, A.M., 2018. The age and tectonic setting of the Lukinda dunite-gabbro-anorthosite massif in the east of the Selenga-Stanovoi superterrane, Central Asian Fold Belt. Russian Geology and Geophysics (Geologiya i Geofizika) 59 (7), 709–717 (889–899).

Cullers, R.L., 2002. Implications of elemental concentrations for provenance, redox conditions, and metamorphic studies of shales and limestones near Pueblo, CO, USA. Chem. Geol. 191, 305–327.

Demonterova, E.I., Ivanov, A.V., Mikheeva, E.A., Arzhannikova, A.V., Frolov, A.O., Arzannikov, S.G., Bryanskiy, N.V., Pavlova, L.A., 2017. Early to Middle Jurassic history of the southern Siberian continent (Transbaikalia) recorded in sediments of the Siberian Craton: Sm–Nd and U–Pb provenance study. Bull. Soc. Géol. Fr. 188 (1–2), 1–29.

Didenko, A.N., Kaplun, V.B., Malyshev, Yu.F., Shevchenko, B.F., 2010. Lithospheric structure and Mesozoic geodynamics of the eastern Central Asian orogen. Russian Geology and Geophysics (Geologiya i Geofizika) 51 (5), 492–506 (629–647).

Donskaya, T.V., Windley, B.F., Mazukabzov, A.M., Kroner, A., Sklyarov, E.V., Gladkochub, D.P., Ponomarchuk, V.A., Badarch, G., Reichow, M.K., Hegner, E., 2008. Age and evolution of Late Mesozoic metamorphic core complexes in southern Siberia and northern Mongolia. J. Geol. Soc. London 165, 405–421.

Donskaya, T.V., Gladkochub, D.P., Mazukabzov, A.M., De Waele, B., Presnyakov, S.L., 2012. The Late Triassic Kataev volcanoplutonic association in western Transbaikalia, a fragment of the active continental margin of the Mongol-Okhotsk Ocean. Russian Geology and Geophysics (Geologiya i Geofizika) 53 (1), 22–36 (30–49).

Donskaya, T.V., Gladkochub, D.P., Mazukabzov, A.M., Ivanov, A.V., 2013. Late Paleozoic–Mesozoic subduction-related magmatism at the southern margin of the Siberian continent and the 150-million-year history of the Mongol–Okhotsk Ocean. J. Asian Earth Sci. 62, 79–97.

Gehrels, G.E., Valencia, V., Ruiz, J., 2008. Enhanced precision, accuracy, efficiency, and spatial resolution of U–Pb ages by laser ablation-multicollector-inductively coupled plasma-mass spectrometry. Geochem. Geophys. Geosyst. 9 (3), 1–13.

Godzevich, B.L., 1984. Geological Map of the Baikal–Amur Railroad Region. Scale 1:500,000. Sheet N-52-A [in Russian]. VSEGEI, Leningrad.

Gou, J., Sun, D.Y., Liu, Y.J., Ren, Y.S., Zhao, Z.H., Liu, X.M., 2013. Geochronology, petrogenesis, and tectonic setting of Mesozoic volcanic rocks, southern Manzhouli area, Inner Mongolia. Int. Geol. Rev. 55 (8), 1029–1048.

Griffin, W.L., Belousova, E.A., Shee, S.R., Pearson, N.J., O'Reilly, S.Y., 2004. Archean crustal evolution in the northern Yilgarn Craton: U–Pb and Hf-isotope evidence from detrital zircons. Precambrian Res. 131, 231–282.

Guo, Z.H., Yang, Y.T., Zyabrev, S., Hou, Z.H., 2017. Tectonostratigraphic evolution of the Mohe–Upper Amur Basin reflects the final closure of the Mongol–Okhotsk Ocean in the latest Jurassic–earliest Cretaceous. J. Asian Earth Sci. 45, 494–511.

Halim, N., Kravchinsky, V., Gilder, S., Cogne, J.-P., Alexutin, M., Sorokin, A., Courtillot, V., Chen, Y., 1998. A palaeomagnetic study from the Mongol–Okhotsk region: rotated Early Cretaceous volcanics and remagnetized Mesozoic sediments. Earth Planet. Sci. Lett. 159, 133–145.

Herron, M.M., 1988. Geochemical classification of terrigenous sands and shales from core or log data. J. Sediment. Petrol. 58, 820–829.

Khanchuk, A.I. (Ed.), 2006. Geodynamics, Magmatism, and Metallogeny of Eastern Russia [in Russian]. Dal'nauka, Vladivostok, Book 1.

Khanchuk, A.I., Didenko, A.N., Popeko, L.I., Sorokin, A.A., Shevchenko, B.F., 2015. Structure and evolution of the Mongol–Okhotsk orogenic belt, in: Kröner, A. (Ed.), The Central Asian orogenic belt. Geology, Evolution, Tectonics, and Models. Borntraeger Science Publishers, Stuttgart, pp. 211–234.

Koshelenko, V.V., 2011. State Geological Map of the Russian Federation. Second Edition. Stanovoi Group. Sheet N-51-XVII [in Russian]. VSEGEI, St. Petersburg.

Kotov, A.B., Sorokin, A.A., Sal'nikova, E.B., Sorokin, A.P., Larin, A.M., Velikoslavinskii, S.D., Belyakov, T.V., Anisimova, I.V., Yakovleva, S.Z., 2009. Mesozoic age of granitoids from the Beket complex (Gonzha block within the Argun terrane of the Central-Asian Fold Belt). Dokl. Earth Sci. 429 (2), 1457–1461.

Kotov, A.B., Larin, A.M., Salnikova, E.B., Velikoslavinskii, S.D., Sorokin, A.A., Sorokin, A.P., Yakovleva, S.Z., Anisimova, I.V., Tolmacheva, E.V., 2012. Tok–Algoma magmatic complex of the Selenga–Stanovoi Superterrain in the Central Asian fold belt: Age and tectonic setting. Dokl. Earth Sci. 444 (1), 562–567.

Kotov, A.B., Mazukabzov, A.M., Skovitina, T.M., Velikoslavinsky, S.D., Sorokin, A.A., Sorokin, A.P., 2013. Structural evolution and geodynamic position of the Gonzha block, Upper Amur region. Geotectonics 47 (5), 351–361.

Kotov, A.B., Larin, A.M., Sal'nikova, E.B., Velikoslavinskii, S.D., Glebovitskii, V.A., Sorokin, A.A., Yakovleva, S.Z., Anisimova, I.V., 2014. Early Cretaceous collisional granitoids of the Drevnestanovoi complex from the Selenga-Stanovoi superterrane of the Central Asian mobile belt. Dokl. Earth Sci. 456 (2), 649–654.

Kozlov, V.D., Efremov, S.V., Dril', S.I., Sandimirova, G.P., 2003. Geochemistry, isotopic geochronology, and genesis of the Verkhnyaya Unda granitoid batholith. Geochem. Int. 41 (4), 364–378.

Kravchinsky, V.A., Sorokin, A.A., Courtillot, V., 2002. Paleomagnetism of Paleozoic and Mesozoic sediments of southern margin of Mongol–Okhotsk ocean, far eastern Russia. J. Geophys. Res. Solid Earth 10, 1–22.

Larin, A.M., Sal'nikova, E.B., Kotov, A.B., Glebovitsky, V.A., Velikoslavinsky, S.D., Sorokin, A.A., Yakovleva, S.Z., Fedoseenko, A.M., Anisimova, I.V., 2006. Early Cretaceous age of regional metamorphism of the Stanovoi group in the Dzhugdzhur-Stanovoi foldbelt: Geodynamic implications. Dokl. Earth Sci. 409 (1), 727–731.

Larin, A.M., Kotov, A.B., Sal'nikova, E.B., Sorokin, A.A., Sorokin, A.P., Korshunov, A.M., Velikoslavinskii, S.D., Yakovleva, S.Z., Plotkina, Yu.V., 2011. Age and tectonic position of granites and volcanics in the eastern Margin of the Selenga-Vitim volcanoplutonic belt. Dokl. Earth Sci. 441 (1), 1502–1507.

Larin, A.M., Kotov, A.B., Sal'nikova, E.B., Velikoslavinskii, S.D., Sorokin, A.A., Sorokin, A.P., Yakovleva, S.Z., Anisimova, I.V., 2014. Granitoids of the Tukuringra complex in the Selenga–Stanovoi superterrane of the Central Asian mobile belt: Age and geodynamic setting. Dokl. Earth Sci. 457 (2), 945–949.

Larin, A.M., Kotov, A.B., Kovach, V.P., Sal'nikova, E.B., Yarmolyuk, V.V., Velikoslavinskii, S.D., Yakovleva, S.Z., Plotkina, Yu.V., 2015. Granitoids of the Olekma Complex in the Selenga–Stanovoi superterrane of the central Asian mobile belt: Age and tectonic position. Dokl. Earth Sci. 464 (1), 903–906.

Ludwig, K.R., 2008. Isoplot 3.6: Berkeley Geochronology Center Special Publication, No. 4.

Maslov, A.V., Mizens, G.A., Podkovyrov, V.N., Gareev, E.Z., Sorokin A.A., Smirnova, Yu.N., Sokur, T.M., 2013. Synorogenic psammites: major lithochemical features. Lithol. Mineral Resour. 48 (1), 74–97.

Maslov, A.V., Mizens, G.A., Podkovyrov, V.N., Nozhkin, A.D., Sokur, T.M., Malinovskii, A.I., Sorokin, A.A., Smirnova, Yu.N., Gareev, E.Z., Dmitrieva, N.V., Krupenin, M.T., Letnikova, E.F., 2015. Synorogenic clay rocks: specifics of bulk composition and paleotectonics. Geochem. Int. 53 (6), 510–533.

Mattinson, J.M., 2010. Analysis of the relative decay constants of ^{235}U and ^{238}U by multi-step CA-TIMS measurements of closed system natural zircon samples. Chem. Geol. 275, 186–198.

McDonough, W.F., Sun, S.S., 1995. The composition of the Earth. Chem. Geol. 120, 223–253.

McLennan, S.M., Hemming, S., McDanniel, D.K., Hanson, G.N., 1993. Geochemical approaches to sedimentation, provenance, and tectonics, in: Johnsson, M.J., Basu, A., Controlling the Composition of Clastic Sediments. Geol. Soc. Am. Spec. Pap. No. 285, 21–40.

Metelkin, D.V., Gordienko, I.V., Zhao, X., 2004. Paleomagnetism of Early Cretaceous volcanic rocks from Transbaikalia: argument for Mesozoic strike-slip motions in Central Asian structure. Geologiya i Geofizika (Russian Geology and Geophysics) 45 (12), 1404–1417 (1349–1363).

Metelkin, D.V., Gordienko, I.V., Klimuk, V.S., 2007. Paleomagnetism of Upper Jurassic basalts from Transbaikalia: new data on the time of closure of the Mongol–Okhotsk Ocean and Mesozoic intraplate teconics of Central Asia. Russian Geology and Geophysics (Geologiya i Geofizika) 48 (10), 825–834 (1061–1073).

Metelkin, D.V., Vernikovsky, V.A., Kazansky, A.Yu., Wingate, M.T.D., 2010. Late Mesozoic tectonics of Central Asia based on paleomagnetic evidence. Gondwana Res. 18, 400–419.

Paces, J.B., Miller, J.D., 1993. Precise U–Pb ages of Duluth Complex and related mafic intrusions, northeastern Minnesota: Geochronological insights to physical, petrogenic, paleomagnetic, and tectonomagmatic processes associated with the 1.1. Ga Midcontinent Rift System. J. Geophys. 98 (8), 13997–14013.

Parfenov, L.M., Popeko, L.I., Tomurtogoo, O., 1999. Problems of the tectonics of the Mongol–Okhotsk orogenic belt. Tikhookeanskaya Geologiya 18 (5), 24–43.

Petruk, N.N., Kozlov, S.A., 2009. State Geological Map of the Russian Federation. Scale 1 : 1,000,000. Sheet N-51 (Skovorodino). The Third Generation. Far East Series [in Russian]. VSEGEI, St. Petersburg.

Pettijohn, F.J., Potter, P.E., Siever, R., 1972. Sands and Sandstone. Springer-Verlag, New York.

Ren, Q., Zhang, S., Wu, H., Liang, Z., Miao, X., Zhao, H., Li, H., Yang, T., Pei, J., Davis, G.A., 2016. Further paleomagnetic results from the ~155 Ma Tiaojishan Formation, Yanshan Belt, North China, and their implications for the tectonic evolution of the Mongol–Okhotsk suture. Gondwana Res. 35, 180–191.

Resolutions of the Fourth Interdepartmental Regional Stratigraphic Workshop on the Precambrian and Phanerozoic of the Southern Far East and Eastern Transbaikalia. A Set of Schemes [in Russian], 1994. KhGGGP, Khabarovsk.

Sal'nikova, E.B., Larin, A.M., Kotov, A.B., Sorokin, A.P., Sorokin, A.A., Velikoslavinsky, S.D., Yakovleva, S.Z., Fedoseenko, A.M., Plotkina, Yu.V., 2006. The Toksko–Algomin igneous complex of the Dzhugdzhur–Stanovoi folded region: Age and geodynamic setting. Dokl. Earth Sci. 409 (2), 888–892.

Serezhnikov, A.N., Volkova, Yu.R., 2007. State Geological Map of the Russian Federation. Scale 1 : 1,000,000. The Third Generation. Sheet N-52 (Zeya). Far East Series [in Russian]. VSEGEI, St. Petersburg.

Smirnova, Yu.N., Sorokin, A.A., Popeko, L.I., Kotov, A.B., Kovach, V.P., 2017. Geochemistry and provenances of the Jurassic terrigenous rocks of the Upper Amur and Zeya–Dep troughs, eastern Central Asian Fold Belt. Geochem. Int. 55 (2), 163–183.

Söderlund, U., Patchett, P.J., Vervoort, J.D., Isachsen, C.E., 2004. The ^{176}Lu decay constant determined by Lu–Hf and U–Pb isotope systematics of Precambrian mafic intrusions. Earth Planet. Sci. Lett. 219, 311–324.

Sorokin, A.A., Kudryashov, N.M., Sorokin, A.P., Rublev, A.G., Levchenkov, O.A., Kotov, A.B., Sal'nikova, E.B., Kovach, V.P., 2003. Geochronology, geochemistry, and geodynamic setting of Paleozoic granitoids in the eastern segment of Mongol–Okhotsk Belt. Dokl. Earth Sci. 393 (8), 1136–1140.

Sorokin, A.A., Kotov, A.B., Kudryashov, N.M., Kovach, V.P., 2005. Late Paleozoic Urusha magmatic complex in the southern framing of the Mongolia–Okhotsk Belt (Amur Region): Age and geodynamic setting. Petrology 13 (6), 596–610.

Sorokin, A.A., Kotov, A.B., Sal'nikova, E.B., Kudryashov, N.M., Kovach, V.P., 2007. Early Paleozoic gabbro–granitoid associations in eastern segment of the Mongolian–Okhotsk Foldbelt (Amur River basin): age and tectonic position. Stratigr. Geol. Correl. 15 (3), 241–257.

Sorokin, A.A., Ponomarchuk, A.V., Travin, A.V., Ponomarchuk, V.A., Vakhtomin, K.D., 2014. New ^{40}Ar/^{39}Ar age of granitic rocks and related gold mineralization at the Kirovskoye deposit (southeastern margin of the North Asian craton). Dokl. Earth Sci. 458 (1), 1230–1235.

Sorokin, A.A., Sorokin, A.P., Ponomarchuk, V.A., Vakhtomin, K.D., 2015a. Early Jurassic volcanics of the Uda belt (Southeastern part of the North Asian Craton): ^{40}Ar/^{39}Ar geochronological and geochemical data. Dokl. Earth Sci. 460 (1), 6–10.

Sorokin, A.A., Kolesnikov, A.A., Kotov, A.B., Sorokin, A.P., Kovach, V.P., 2015b. Sources of detrital zircons from terrigenous deposits in the Yankan terrane of the Mongolian-Okhotsk mobile belt. Dokl. Earth Sci. 462 (2), 621–625.

Sorokin, A.A., Xu, B., Sorokin, A.P., Zaika, V.A., Plyaskin, Yu.V., 2017. Early Mesozoic age of protolites of metasedimentary rocks from the Tukuringra terrane in the Mongolian–Okhotsk fold belt: Results of LA–ICP–MS U–Pb geochronological studies. Dokl. Earth Sci. 474 (1), 542–545.

Stacey, J.S., Kramers, I.D., 1975. Approximation of terrestrial lead isotope evolution by a two-stage model. Earth Planet. Sci. Lett. 26 (2), 207–221.

Sun, D.Y., Gou, J., Wang, T.H., 2013. Geochronological and geochemical constraints on the Erguna massif basement, NE China, subduction history of the Mongol–Okhotsk oceanic crust. Int. Geol. Rev. 55 (14), 1801–1816.

Tang, J., Xu, W.L., Wang, F., Zhao, S., Li, Y., 2015. Geochronology, geochemistry, and deformation history of Late Jurassic–Early Cretaceous intrusive rocks in the Erguna Massif, NE China: Constraints on the late Mesozoic tectonic evolution of the Mongol–Okhotsk orogenic belt. Tectonophysics 658, 91–110.

Tang, J., Xu, W.L., Wang, F., Zhao, S., Wang, W., 2016. Early Mesozoic southward subduction history of the Mongol–Okhotsk oceanic plate: Evidence from geochronology and geochemistry of Early Mesozoic intrusive rocks in the Erguna Massif, NE China. Gondwana Res. 31, 218–240.

Taylor, S.R., McLennan, S.M., 1985. The Continental Crust: Its Composition and Evolution. Blackwell, Oxford.

Tsygankov, A.A., Livtinovsky, B.A., Jahn, B.M., Reichow, M.K., Liu, D.Y., Larionov, A.N., Presnyakov, S.L., Lepekhina, Ye.N., Sergeev, S.A., 2010. Sequence of magmatic events in the Late Paleozoic of Transbaikalia, Russia (U-Pb isotope data). Russian Geology and Geophysics (Geologiya i Geofizika) 51 (9), 972–994 (1249–1276).

Velikoslavinskii, S.D., Kotov, A.B., Sal'nikova, E.B., Larin, A.M., Sorokin, A.A., Sorokin, A.P., Kovach, V.P., Tolmacheva, E.V., Gorokhovskii, B.M., 2011. Age of the Ilikan sequence from the Stanovoi complex of the Dzhugdzhur–Stanovoi superterrane, Central-Asian Foldbelt. Dokl. Earth Sci. 438 (1), 612–616.

Velikoslavinskii, S.D., Kotov, A.B., Salnikova, E.B., Larin, A.M., Sorokin, A.A., Sorokin, A.P., Kovach, V.P., Tolmacheva, E.V., Yakovleva, S.Z., Anisimova, I.V., 2012a. Age of the Ust'-Gilyui sequence in the Stanovoi complex of the Selenga–Stanovoi superterrain, Central Asian fold belt. Dokl. Earth Sci. 444 (2), 661–665.

Velikoslavinskii, S.D., Kotov, A.B., Kovach, V.P., Tolmacheva, E.V., Larin, A.M., Sorokin, A.A., Sorokin, A.P., Wang, K.L., Salnikova, E.B., 2016a. Age, sources, and provenances of protoliths of metasedimentary rocks of the Dzheltulak group, Dzheltulak suture. Dokl. Earth Sci. 468 (2), 545–548.

Velikoslavinskii, S.D., Kotov, A.B., Kovach, V.P., Larin, A.M., Sorokin, A.A., Sorokin, A.P., Tolmacheva, E.V., Salnikova, E.B., Wang, K.L., Jahn, B.M., Chung, S.L., 2016b. Mesozoic age of the Gilyui Metamorphic Complex in the junction zone of the Selenga–Stanovoi and Dzhugdzhur–Stanovoi superterranes, Central Asian fold belt. Dokl. Earth Sci. 468 (2), 561–565.

Velikoslavinskii, S.D., Kotov, A.B., Kovach, V.P., Tolmacheva, E.V., Sorokin, A.A., Sal'nikova, E.B., Larin, A.M., Zagornaya, N.Yu., Wang, K.L., Chung, S.-L., Yarmolyuk, V.V., Kheraskova, T.N., 2017. Age and tectonic position of the Stanovoi metamorphic complex in the eastern part of the Central Asian Foldbelt. Geotectonics 51 (4), 341–352.

Velikoslavinsky, S.D., Kotov, A.B., Salnikova, E.B., Sorokin, A.A., Larin, A.M., Yakovleva, S.Z., Kovach, V.P., Tolmacheva, E.V., Anisimova, I.V., Plotkina, Yu.V., Sorokin, A.A., 2012b. Metabasalts of the Bryanta sequence of the Stanovoi complex of the Dzhugdzhur–Stanovoi superterrane, Central Asian Fold Belt: Age and geodynamic environment of formation. Petrology 20 (3), 240–254.

Vervoort, J.D., Patchett, P.J., 1996. Behavior of hafnium and neodymium isotopes in the crust: constraints from Precambrian crustally derived granites. Geochim. Cosmochim. Acta 60, 3717–3723.

Vol'skii, A.S., Afanasov, M.N., Godzevich, B.L., El'yanov, A.A., Kastrykina, V.M., Kastrykin, Yu.P., 1984. Geological Map of the Baikal–Amur Railroad Region. Scale 1:500,000. Sheet N-51-B [in Russian]. VSEGEI, Leningrad.

Wang, T., Tong, Y., Zhang, L., Li, S., Huang, H., Jianjun Zhang, J., Guo, L., Yang, Q., Hong, D., Donskaya, T., Gladkochub, D., Tserendash, N., 2017. Phanerozoic granitoids in the central and eastern parts of Central Asia and their tectonic significance. J. Asian Earth Sci. 145, 368–392.

Wu, L., Kravchinsky, V.A., Gu, Y.J., Potter, D.K., 2017. Absolute reconstruction of the closing of the Mongol–Okhotsk Ocean in the Mesozoic elucidates the genesis of the slab geometry underneath Eurasia. J. Geophys. Res. Solid Earth 122 (7), 4831–4851.

Yang, Y.T., Guo, Z.X., Song, C.C., Li, X.B., He, S., 2015. A short-lived but significant Mongol–Okhotsk collisional orogeny in latest Jurassic–earliest Cretaceous. Gondwana Res. 28, 1096–1116.

Zaika, V.A., Sorokin, A.A., Xu, B., Kotov, A.B., Kovach, V.P., 2018. Geochemical features and sources of metasedimentary rocks of the western part of the Tukuringra terrane of the Mongol–Okhotsk Fold Belt. Stratigr. Geol. Correl. 26 (2), 157–178.

Zaika, V.A., Sorokin, A.A., Kovach, V.P., Sorokin, A.P., Kotov, A.B., 2019. Age and sources of Lower Mesozoic metasedimentary rocks of the Un'ya–Bom terrane in the Mongol–Okhotsk Fold Belt: results of U–Pb geochronological (LA-ICP-MS) and Sm–Nd isotope studies. Dokl. Earth Sci. 484 (2), 115–119.

Zhao, X., Coe, R., Zhou, Y., Wu, H., Kuang, G., Wang, J., 1994. Tertiary paleomagnetism of North and South China and reappraisal of Late Mesozoic paleomagnetic data from Eurasia: implications for the Cenozoic tectonic history of Asia. Tectonophysics. 235, 181–203.

Editorial responsibility: E.V. Sklyarov